Monthly Notices
of the
ROYAL ASTRONOMICAL SOCIETY

Mon. Not. R. Astron. Soc. **422,** 2164–2186 (2012) doi:10.1111/j.1365-2966.2012.20760.x

Observing supermassive dark stars with *James Webb Space Telescope*

Cosmin Ilie,[1⋆] Katherine Freese,[1,2] Monica Valluri,[3] Ilian T. Iliev[4] and Paul R. Shapiro[2,5]

[1]*Michigan Center for Theoretical Physics, Physics Department, University of Michigan, Ann Arbor, MI 48109, USA*
[2]*Texas Cosmology Center, University of Texas, Austin, TX 78712, USA*
[3]*Department of Astronomy, University of Michigan, Ann Arbor, MI 49109, USA*
[4]*Department of Physics & Astronomy, University of Sussex, Brighton BN1 9QH*
[5]*Department of Astronomy, University of Texas, Austin, TX 78712, USA*

Accepted 2012 February 15. Received 2012 February 13; in original form 2011 October 27

ABSTRACT

We study the capability of the*James Webb Space Telescope* (*JWST*) to detect supermassive dark stars (SMDSs). If the first stars are powered by dark matter (DM) heating in triaxial DM haloes, they may grow to be very large ($>10^6\,M_\odot$) and very bright ($>10^9\,L_\odot$). These SMDSs would be visible in deep imaging with *JWST* and even *Hubble Space Telescope* (*HST*). We use sensitivity limits from previous *HST* surveys to place bounds on the numbers of SMDSs that may be detected in future *JWST* imaging surveys. We showed that SMDS in the mass range 10^6–$10^7\,M_\odot$ are bright enough to be detected in all the wavelength bands of the NIRCam on *JWST* (but not in the less sensitive MIRI camera at higher wavelengths). If SMDSs exist at $z\sim 10$, 12 and 14, they will be detectable as *J*-, *H*- or *K*-band dropouts, respectively. With a total survey area of 150 arcmin^2 (assuming a multiyear deep parallel survey with *JWST*), we find that typically the number of $10^6\,M_\odot$ SMDSs found as *H*- or *K*-band dropouts is $\sim 10^5\,f_{\rm SMDS}$, where the fraction of early DM haloes hosting DS is likely to be small, $f_{\rm SMDS}\ll 1$. If the SMDS survive down to $z=10$ where *HST* bounds apply, then the observable number of SMDSs as *H*- or *K*-band dropouts with *JWST* is ∼1–30. While individual SMDS are bright enough to be detected by *JWST*, standard Population III stars (without DM annihilation) are not, and would only be detected in first galaxies with total stellar masses of 10^6–$10^8\,M_\odot$. Differentiating first galaxies at $z>10$ from SMDSs would be possible with spectroscopy: the SMDS (which are too cool produce significant nebular emission) will have only absorption lines, while the galaxies are likely to produce emission lines as well. Of particular interest would be the He II emission lines at $\lambda\sim 1.6\,\mu$m as well as Hα lines which would be signatures of early galaxies rather than SMDSs. The detection of SMDSs with *JWST* would not only provide alternative evidence for weakly interacting massive particles, but also provide a possible pathway for the formation of massive (10^4–$10^6\,M_\odot$) seeds for the formation of supermassive black holes that power quasi-stellar objects at $z=6$.

Key words: stars: Population III – stars: pre-main-sequence – galaxies: high-redshift – dark ages, reionization, first stars – dark matter.

1 INTRODUCTION

The first stars are thought to have formed at $z=10$–50 when the Universe was about 200 million years old in $\sim 10^6\,M_\odot$ (mini) haloes consisting of 85 per cent dark matter (DM) and 15 per cent baryons in the form of H and He from big bang nucleosynthesis. Their formation marks the end of the 'dark ages' of the Universe. For reviews of the standard picture of the formation of the first stars, see Barkana & Loeb (2001), Yoshida et al. (2003), Bromm & Larson (2004), Ripamonti & Abel (2005) and Bromm et al. (2009).

Spolyar, Freese & Gondolo (2008) first showed that DM heating may drastically alter the picture of formation for these first stars. The canonical example of particle DM is weakly interacting massive particles (WIMPs). In many theories, WIMPs are their own antiparticles and annihilate with themselves wherever the DM density is high. In fact, this annihilation process is exactly what is responsible in the early Universe for leaving behind the correct relic WIMP abundance today to solve the DM problem, 24 per cent of the energy density of the Universe. The same annihilation process would then take place also in the collapsing protostellar clouds

⋆E-mail: cilie@umich.edu

at the centres of minihaloes. At suitably high baryonic density in these clouds, the annihilation products get stuck inside the cloud and prevent it from undergoing further collapse. The annihilation products thermalize with the baryons and provide a very powerful heat source. Indeed, the object becomes a 'dark star' (DS), which, despite its name, shines very bright. The DM – while only a negligible fraction of the star's mass – provides the key power source for the star through DM heating. Note that the term 'dark' refers to the power source, not the content of the star. These first DSs are stars made primarily of hydrogen and helium with a smattering of DM (<1 per cent of the mass consists of DM); yet they shine due to DM heating.

Recently, there has been much excitement in the DM community about hints of WIMP detections in a number of experiments: excess positrons in the *PAMELA* satellite (Adriani et al. 2009, 2010; Abdo et al. 2010) may be due to DM annihilation (though alternative astrophysical explanations are more likely). Excess γ-rays in the *Fermi* satellite (Abdo et al. 2009a,b; Dobler et al. 2010; The Fermi LAT Collaboration 2011) may be due to DM annihilation, and annual modulation (Drukier, Freese & Spergel 1986; Freese, Frieman & Gould 1988) in direct detection experiments DAMA (Bernabei et al. 2010) and COGENT (Aalseth et al. 2011). The CRESST experiment (Angloher et al. 2011) also has unexplained events.

The WIMP annihilation rate is $n_\chi^2 \langle \sigma v \rangle$, where n_χ is WIMP density and we take the standard annihilation cross-section

$$\langle \sigma v \rangle = 3 \times 10^{-26}\,\mathrm{cm^3\,s^{-1}}, \quad (1)$$

and WIMP masses in the range 1 GeV–10 TeV. WIMP annihilation produces energy at a rate per unit volume

$$\hat{Q}_{\rm DM} = n_\chi^2 \langle \sigma v \rangle m_\chi = \langle \sigma v \rangle \rho_\chi^2 / m_\chi, \quad (2)$$

where n_χ is the WIMP number density, m_χ is the WIMP mass and ρ_χ is the WIMP energy density. The annihilation products typically are electrons, photons and neutrinos. The neutrinos escape the star, while the other annihilation products are trapped in the DS, thermalize with the star and heat it up. The luminosity from the DM heating is

$$L_{\rm DM} \sim f_Q \int \hat{Q}_{\rm DM} {\rm d}V, \quad (3)$$

where f_Q is the fraction of the annihilation energy deposited in the star (not lost to neutrinos) and dV is the volume element. We take $f_Q = 2/3$ as is typical for WIMPs.

DSs are born with masses $\sim$1 M$_\odot$. They are giant puffy ($\sim$10 au), cool (surface temperatures <10 000 K), yet bright objects (Freese et al. 2008a). They reside in a large reservoir ($\sim 10^5$ M$_\odot$) of baryons, i.e. $\sim$15 per cent of the total halo mass. These baryons can start to accrete on to the DSs. DSs can continue to grow in mass as long as there is a supply of DM fuel. We consider two different mechanisms that can continually provide the requisite DM fuel, allowing them to become supermassive DSs (SMDS) of mass $M_{\rm DS} > 10^5$ M$_\odot$.

(1) *Extended adiabatic contraction (AC)*. The central DM density is enhanced due to an increase in the depth of the gravitation potential well due to the infall of baryons. We treat this gravitational effect via the Blumenthal method for AC. While this approach is simple to implement, we (Freese et al. 2009) and others (Iocco et al. 2008; Natarajan, Tan & O'Shea 2009) have previously shown that it provides DM densities accurate to within a factor of 2, which is perfectly adequate for these studies. In the central cusps of triaxial DM haloes, DM particles follow a variety of centrophilic orbits (box orbits and chaotic orbits; Valluri et al. 2010) whose population is continuously replenished, allowing DM annihilation to continue much longer than in spherical DM haloes. The period of extended AC can thus last for a very long time (hundreds of millions of years or more). Freese et al. (2010a) showed that this replenishment of the DM in the central cusp could be used to followed the growth of DSs from their inception at 1 M$_\odot$, till they become SMDS of mass $M_{\rm DS} > 10^5$ M$_\odot$.

(2) *Capture*. As a second mechanism for DM refuelling, we take the star to be initially powered by the DM from AC, but assume the AC phase is short, $\sim$300 000 yr; once this DM runs out, the star shrinks, its density increases, and subsequently the DM is replenished inside the star by capture of DM from the surroundings (Freese, Spolyar & Aguirre 2008b; Iocco 2008; Sivertsson & Gondolo 2011) as it scatters elastically off of nuclei in the star. In this case, the additional particle physics ingredient of WIMP scattering is required. This elastic scattering is the same mechanism that direct detection experiments (e.g. CDMS, XENON, LUX, DAMA, COGENT, COUPP, CRESST) are using in their hunt for WIMPs.

SMDSs can result from either of these mechanisms for DM refuelling inside the star. Umeda et al. (2009) considered a different scenario which also results in SMDSs. In all of these cases, SMDSs can live for a very long time, tens to hundreds of million years, or possibly longer (even to today). We find that SMDS of mass $M_{\rm DS} > 10^6$ M$_\odot$ SMDSs are very bright, $>3 \times 10^9$ L$_\odot$, which makes them potentially observable by the *James Webb Space Telescope* (*JWST*).

The key ingredient that allows DSs to grow so much larger than ordinary fusion-powered Population III (Pop III) stars is the fact that DSs are so much cooler. Ordinary Pop III stars have much larger surface temperatures in excess of 50 000 K. They produce ionizing photons that provide a variety of feedback mechanisms that cut off further accretion. McKee & Tan (2008) have estimated that the resultant Pop III stellar masses are $\sim$140 M$_\odot$. The issue of the initial mass function (IMF) for Pop III stars is far from being solved. Recent simulations (see Clark et al. 2011; Greif et al. 2011a,b) indicate that the typical mass of such objects is much lower that previously thought. DSs are very different from fusion-powered stars, and their cooler surface temperatures allow continued accretion of baryons all the way up to enormous stellar masses, $M_{\rm DS} > 10^5$ M$_\odot$.

In this paper, we discuss detectability of these objects in the upcoming *JWST*. In future work, we will investigate how well other observations with *Herschel*, *Spitzer*, Giant Magellan Telescope (GMT), Thirty Meter Telescope (TMT) and other instruments can detect or place bounds on DSs. We restrict our discussion only to SMDS of mass 10^6–10^7 M$_\odot$ (we show that SMDS of 10^5 and lower are hard to detect). Previously, Zackrisson et al. (2010a) studied DSs of even lower masses, and concluded that even $\lesssim 10^3$ M$_\odot$ DS could be detected as individual objects with *JWST* if their fluxes were magnified by gravitational lensing by a well-placed foreground cluster. Since SMDS are larger and brighter, they are easier to detect. A preliminary study of detectability with *JWST* and *Hubble Space Telescope* (*HST*) of SMDS was made in Freese et al. (2010a, 2010b). Freese et al. approximated the spectrum of the DS as a pure blackbody determined by its temperature and radius and used it to show that individual SMDS would be detectable with *JWST* and *HST*. In this paper, we improve our estimate by using spectra from the TLUSTY model stellar atmospheres code for zero-metallicity atmospheres from the work of Zackrisson et al. (2010b).

SMDS formed via extended AC are easier to detect than those formed with capture. Those formed 'with capture' are somewhat hotter (by a factor of few) and have radii smaller by a factor of

5–10 for the same stellar mass. Because they are hotter, their peak wavelength moves out of the most sensitive ranges for *HST* and *JWST*, and their fluxes in the detectors are lower.

Once the SMDS run out of DM fuel, they contract and heat up till the core reaches 10^8 K and fusion begins. Due to their extremely large masses, the fusion-powered phase is short and the SMDSs collapse to from massive black holes (BHs) of mass 10^4–10^6 $M_\odot$. Again, this prediction is different from standard Pop III stars, many of which explode as pair-instability supernovae (SNe; Heger & Woosley 2002) with predicted even/odd element abundance ratios that are not (yet) observed in nature. These massive BHs remnants could provide the moderately massive 'seeds' for the formation of nuclear supermassive BHs accounting for the existence of 10^9 $M_\odot$ BHs (Haiman & Loeb 2001) which are the central engines of the most distant ($z \gtrsim 6$) quasars in the Sloan Digital Sky Survey (Fan et al. 2001, 2004, 2006). Indeed, direct collapse of very metal-poor, low-angular momentum gas via dynamical instabilities (Loeb & Rasio 1994; Begelman, Volonteri & Rees 2006; Lodato & Natarajan 2006) has been proposed as a way to form massive 'seed' BHs of 10^4–10^6 $M_\odot$ at redshifts of 10–15. These massive seed formation scenarios, however, are difficult to confirm observationally since the BHs form in compact, low-luminosity cold gas discs and the BH formation is accompanied by a sudden burst with a luminosity of 10^9 $L_\odot$. In contrast, if the 'seeds' form from SMDSs, they may well shine for 10^6–10^7 years prior to their collapse to a BH, enabling them to be detected by *JWST*.

SMDS could also make plausible precursors of intermediate-mass BHs, and account for the BHs inferred by extragalactic radio excess seen by the ARCADE experiment (Seiffert et al. 2009). In addition, the BH remnants from DS could play a role in high-redshift γ-ray bursts thought to take place due to accretion on to early BHs (Narayan, Piran & Kumar 2001).

The possibility that DM annihilation might have effects on *today's* stars was initially considered in the 1980s and early 1990s (Krauss et al. 1985; Press & Spergel 1985; Bouquet & Salati 1989; Salati & Silk 1989) and has recently been studied in interesting papers by Moskalenko & Wai (2007), Scott, Edsjö & Fairbairn (2007), Bertone & Fairbairn (2008), Scott, Fairbairn & Edsjo (2008), Casanellas & Lopes (2009), Hooper et al. (2010) and Scott (2010).

Several authors have explored the repercussions of DM heating in the first stars, including Spolyar et al. (2008, 2009), Freese et al. (2008a, 2008b), Taoso et al. (2008), Yoon, Iocco & Akiyama (2008), Iocco et al. (2008), Ripamonti et al. (2009, 2010), Schleicher, Banerjee & Klessen (2009), Gondolo et al. (2010), Sivertsson & Gondolo (2011), Casanellas & Lopes (2011), Hirano, Umeda & Yoshida (2011), Iocco (2010), Ilie, Freese & Spolyar (2011) and Scott (2010).

The effects of DS (and those of the resultant main-sequence stars) on reionization were studied by Schleicher, Banerjee & Klessen (2008) and Schleicher et al. (2009) and more recently by Scott et al. (2011) as discussed below.

In this paper, we follow the approach taken by Zackrisson et al. (2010b, 2011b). Similar to their work, we use SMDS spectra from the TLUSTY code, compute the formation rate of DSs by counting DM haloes in *N*-body simulations and use *HST* data to bound the numbers of SMDS that survive to $z = 10$ and therefore the numbers that may be seen with *JWST*. Their study focused on 10^7 $M_\odot$ SMDS, while we consider lower mass ones as well. We go beyond their work by studying SMDS as *H*- and *K*-band dropouts with *JWST*, where *JWST* can really improve upon all previous data sets.

Previously, Zackrisson (2011) has noted the possibility that the hottest SMDSs ($T_{\rm eff} > 30\,000$ K) might be able to produce their own H II regions, causing them to be substantially brighter than what estimates based on stellar atmospheres would suggest. Although such a scenario is unlikely (there is not likely to be enough gas left in the halo as it is either eaten by SMDSs or ejected; Alvarez, Bromm & Shapiro 2006), the resulting nebular emission from SMDSs would increase their fluxes by up to 2 mag, making them easier to detect. The SMDS spectra would be modified as well. As discussed below in Section 6, in this paper we do not consider this possible effect and focus instead on the more likely case of no nebular emission. Nevertheless, in the observational search for DSs, the possibility of such enhanced fluxes should be kept in mind.

The paper is organized as follows. In Section 2, we describe the spectra of SMDS obtained by using the TLUSTY code. In Section 3, we compute formation rate of DSs, by counting DM haloes in an *N*-body simulation of structure formation at $z > 10$ carried out with the CUBE P^{3}M code (Iliev et al. 2010) and assuming that some fraction $f_{\rm SMDS}$ of these early haloes will host DS. In Section 4, we examine the detectability of SMDS in *HST*. In fact, *HST* has seen objects out to $z \sim 10$, and it is interesting to speculate that *HST* could already have seen SMDS if they survive to redshift $z = 10$. With current imaging data, it is impossible to differentiate between an early galaxy composed of Pop III stars from an SMDS. However, the fact that *HST* has only seen one object at this high redshift can be used to set bounds (Zackrisson et al. 2010a) the numbers of DSs at $z \sim 10$. In Section 5, we show that DSs may be detected in a variety of *JWST* filters, and in particular may show up as *J*-, *H*- or *K*-band dropouts; such a detection would then give an indication of their redshift. In Section 6, we compare early galaxies at high redshifts (consisting of Pop III stars with different IMFs) with SMDS, which will look very similar with *JWST*, and start a discussion of ways to differentiate between them. In Section 7, we conclude and summarize the results of our study.

2 DARK STAR SPECTRA

In this section, we present spectra of SMDS obtained with the publicly available TLUSTY (Hubeny 1988) synthetic stellar atmospheres code. As discussed in Freese et al. (2010a), SMDS formed via captured DM are much hotter than SMDS formed via extended AC. Also, stars formed via capture undergo a Kelvin–Helmholtz contraction phase prior to DM capture, hence their radii are five to 10 times smaller than those SMDS of the same mass formed via the extended AC mechanism. Since DSs are composed of primordial hydrogen and helium, no other elements are assumed to be present in the atmosphere, and hence all the observed spectral lines are those of H and He. However, the differences in the temperature and radii of SMDS formed via these two mechanisms are responsible for the differences in the spectra in the two panels of Fig. 1. The left-hand panel shows the spectrum for a 10^6 $M_\odot$ DS with surface temperature $T_{\rm eff} = 1.9 \times 10^4$ K which grew via extended AC. The Lyman edge is seen at roughly 0.1 μm.[1] Similarly, Fig. 1 (right) illustrates the spectrum for a 10^6 $M_\odot$ and $T_{\rm eff} = 5.1 \times 10^4$ K DS

[1] Compared to a blackbody of the same temperature, photons below the Lyman edge have typically been shifted to higher wavelengths (lower energy) by absorption and rescattering. However, the excess seen at wavelengths just below the Lyman edge is due to photons coming from deeper inside the star (the photosphere is at roughly an optical depth ~1, and at this wavelength there is very little absorption).

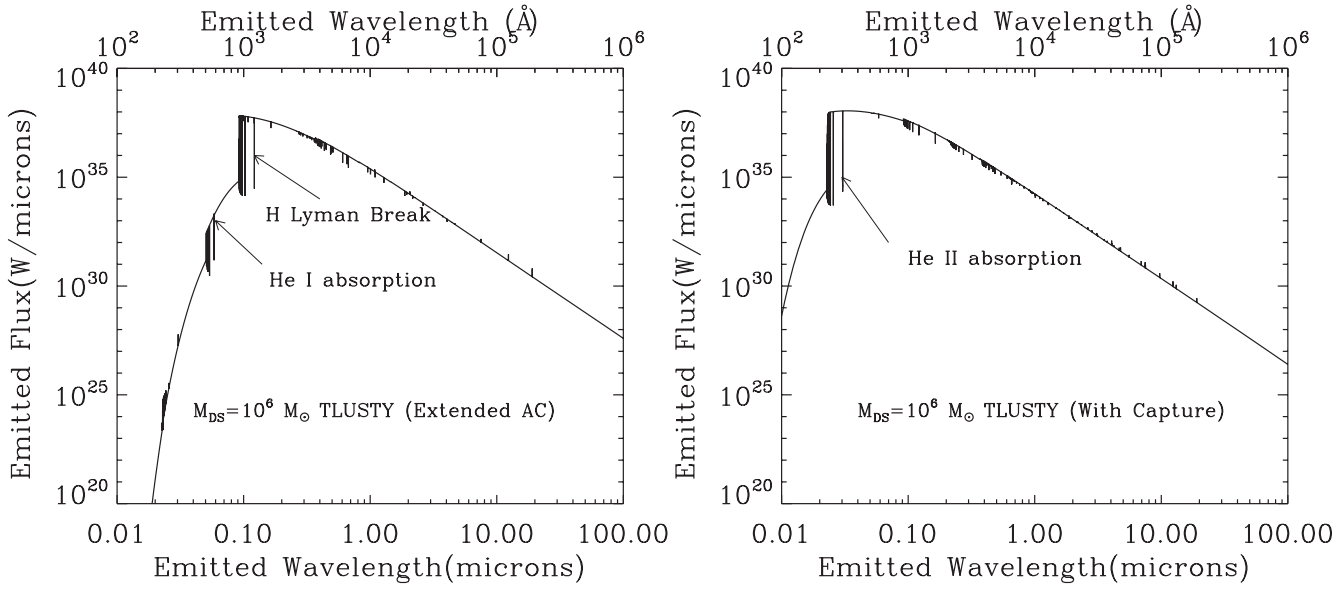

Figure 1. Expected SEDs of 10^6 $M_\odot$ SMDS. Left-hand panel: DS with a surface temperature of 1.9×10^4 K and formed via the extended AC only mechanism. Right-hand panel: with a surface temperature of 5.1×10^4 K and formed 'with capture'.

which grew via captured DM. The most prominent differences from the left-hand panel are a shift of the peak in the spectrum to lower wavelengths and a steeper ultraviolet (UV) continuum slope β ($f_\lambda \propto \lambda^\beta$). Despite the fact that the SMDS formed via capture is hotter, its significantly smaller radius makes it harder to detect in the near-infrared (NIR) at redshifts of $\sim$10 and above.

There are significant differences in the spectra in the two cases. In the left-hand panel (extended AC), the lower surface temperature ($\sim 2 \times 10^4$ K) implies that a significant fraction of neutral H and He remain in the stellar atmosphere, resulting in strong absorption lines at wavelengths corresponding to the Lyman series (0.1216–0.0912 μm). At shorter wavelengths, we note another break in the spectrum due to neutral helium (He I) absorption ($\sim$0.05–0.06 μm). In the right-hand panel ('with capture'), the higher surface temperature ($T_{\rm eff} \sim 5 \times 10^4$ K) implies that H is ionized, hence the Lyman absorption lines are weaker. The break in the spectrum in Fig. 1 right-hand panel corresponds to absorption by singly ionized helium (He II) at wavelengths ranging between 0.023 and 0.030 μm. In the left-hand panel, He I lines appear at wavelengths $\sim$[0.3–0.45 μm], He II lines at wavelengths $\sim$0.46 μm and more He I lines at $\sim$[0.47–0.7 μm]. The same lines, with somewhat weaker strength, are seen in the right-hand panel. In both cases, we note a sequence of absorption lines in $\sim$[0.8–1.0 μm], which correspond to He I absorption.

3 DARK STAR FORMATION RATE

The first DSs can form in the early Universe inside minihaloes of $\sim 10^6$ $M_\odot$, where protostellar clouds collapse via molecular hydrogen cooling until the DM heating sets in. Later in 10^8 $M_\odot$ haloes, where clouds collapse via atomic line radiative cooling, larger DS can form. To compute the detection rate of SMDS with *JWST*, we need to know the formation rate of 10^6–10^8 $M_\odot$ DM haloes. If we assume that a fraction $f_{\rm SMDS}$ of these haloes contain DSs, we can use this to compute the formation rate of DSs. We will attempt to set constraints on this fraction by using the fact that a single $z = 10$ object was observed in recent *HST Ultra Deep Field* observations with the Wide Field Camera 3 (WFC3) (hereafter HUDF09; Bouwens et al. 2011).

A similar study by Zackrisson et al. (2010b, 2011b) for the case of 10^7 $M_\odot$ SMDS concluded that the prior null detection of $z = 10$ objects in first year HUDF09 observation (Bouwens et al. 2010) was sufficient to rule out the detection of 10^7 $M_\odot$ SMDS with *JWST*. However, these authors did not consider the effect of the time it takes the SMDS to grow when computing the formation rates for DM haloes that could host such objects. This effect is transparent in Table 1 in the differences between what we labelled as $z_{\rm start}$ (the redshift that should be used when computing the formation rate of DM haloes) and $z_{\rm form}$ (the redshift when the DS reaches its final mass). Consideration of a finite time required for the SMDS to grow (following the formation of its host DM halo) significantly lowers the bounds predicted from *HST*, since to be visible at $z = 10$ the more massive DM haloes have to formed at a higher redshifts, where they are rarer. In addition, we consider the case of the 10^6 $M_\odot$ SMDS, since these objects are likely to be more numerous, are detectable with *JWST*, and are also subject to bounds from existing *HST* observations.

We use N-body simulations of structure formation at high redshifts from Iliev et al. (2010) carried out with the CUBE P^{3}M N-body code, developed from the particle-mesh PMFAST (Merz, Pen & Trac 2005). This high-resolution simulation considers a comoving volume of $6.3\,h^{-1}$ Mpc with 1728^3 particles of mass 5.19×10^3 $M_\odot$ and hence is able to resolve haloes of mass $\gtrsim 5 \times 10^5$ $M_\odot$. We compute the formation rate (dn/dt as a function of redshift per comoving Mpc^3 per year) of minihaloes with masses within different mass ranges. Fig. 2 shows the formation rate of haloes in two mass ranges that span a factor of 2 in mass (10^7–2×10^7 $M_\odot$ and 10^8–2×10^8 $M_\odot$), while Fig. 3 shows the formation rate of haloes in two mass ranges that span a factor of 5 in mass (10^7–5×10^7 $M_\odot$ and 10^8–5×10^8 $M_\odot$).

We computed the formation rate of DM minihaloes using two different sets of bin widths, to show that the results are relatively insensitive to this issue. As our canonical case, we computed the formation rate dn/dt of minihaloes per Mpc^{-3} yr^{-1} formed in a bin whose width is a factor of 2 in mass (Fig. 2). dn/dt as a function of redshift is shown for haloes in the mass range (1–2) $\times 10^7$ $M_\odot$ (left-hand panel) and for haloes in the mass range (1–2) $\times 10^8$ $M_\odot$

Table 1. DM halo formation rates: dn/dt expressed in $Mpc^{-3}\ yr^{-1}$, and $dN/dz d\theta^2$ as number formed per unit redshift and $arcmin^2$ for cases considered in the text. Top three rows A–C are for a $10^7\ M_\odot$ SMDS forming DM haloes of mass (1–2) $\times\ 10^8\ M_\odot$; bottom three rows are for the $10^6\ M_\odot$ SMDS forming in DM haloes of mass (1–2) $\times\ 10^7\ M_\odot$. We have assumed that the DS started accreting baryons with a constant rate of $10^{-1}\ M_\odot\ yr^{-1}$ at z_{start} and reached its final mass by z_{form}.

Scenario name	Halo mass range ($M_\odot$)	M_{DS} ($M_\odot$)	z_{form}	z_{start}	dn/dt ($Mpc^{-3}\ yr^{-1}$)	$dN/dz d\theta^2$ ($arcmin^{-2}$)
A	(1–2) $\times\ 10^8$	10^7	10	13	5×10^{-9}	235
B	(1–2) $\times\ 10^8$	10^7	12	16	7×10^{-10}	16
C	(1–2) $\times\ 10^8$	10^7	15	22	1×10^{-10}	0.77
A	(1–2) $\times\ 10^7$	10^6	10	10.7	5×10^{-8}	4435
B	(1–2) $\times\ 10^7$	10^6	12	12.8	6×10^{-8}	2965
C	(1–2) $\times\ 10^7$	10^6	15	16	2×10^{-8}	466

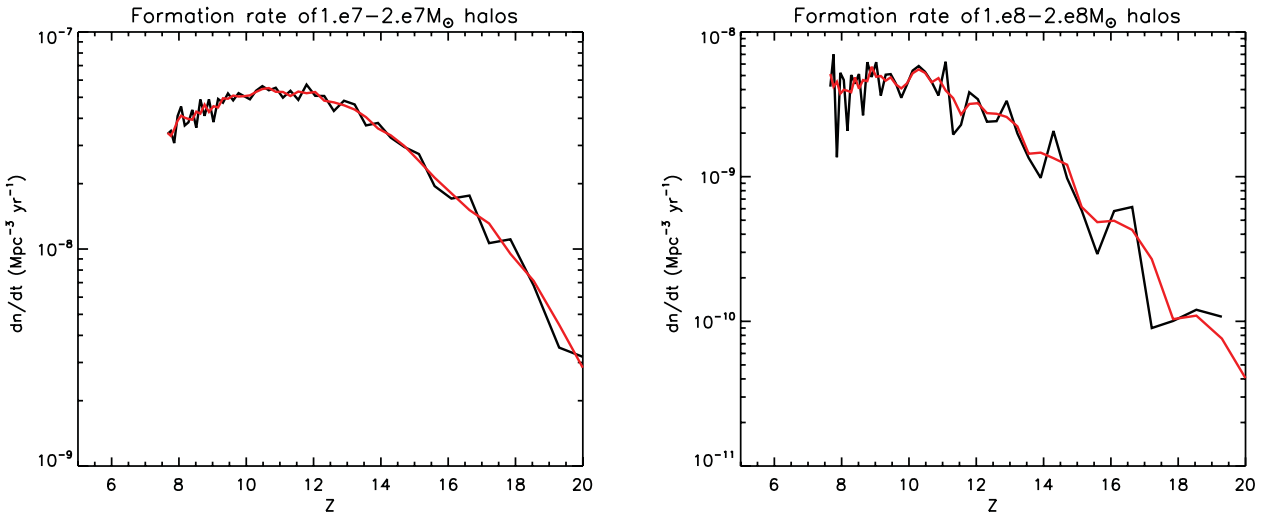

Figure 2. Left: the formation rate of 1–2 $\times\ 10^7\ M_\odot$ minihaloes per comoving Mpc^3 and year. These haloes are potential hosts for the $10^6\ M_\odot$ SMDS. Right: formation rate for 1–2 $\times\ 10^8\ M_\odot$ minihaloes in which a $10^7\ M_\odot$ SMDS can form. The black lines correspond to the formation rate computed directly from the N-body simulation and the smoother red lines (obtained by computing a running average) simply improve visibility of the general trend.

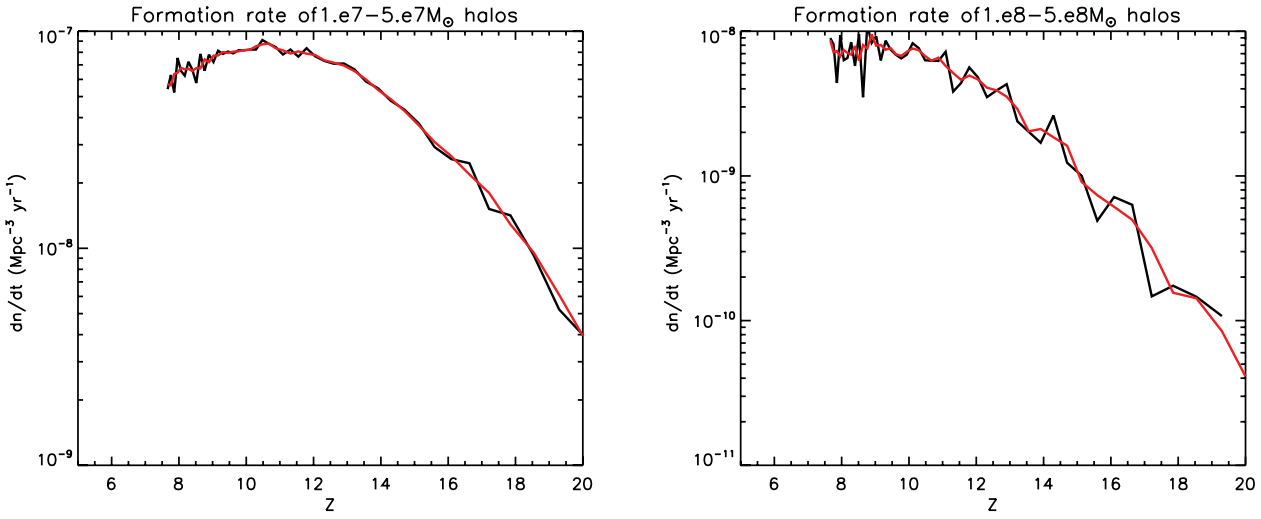

Figure 3. As in Fig. 2, but with the larger mass bin width (see scenario II in text). In the left-hand panel, we plot the formation rate of minihaloes with a mass in the 1–5 $\times\ 10^7\ M_\odot$ range, where a DS of $10^6\ M_\odot$ could form. The panel on the right is for haloes in the 1–5 $\times\ 10^8\ M_\odot$ range, where a DS of $10^7\ M_\odot$ could form.

(right-hand panel). Since the baryonic fraction initially in the halo is roughly 15 per cent, we assume that a DS forming in a halo of a given mass can attain at most 10–15 per cent of the mass of its host halo. Following Freese et al. (2010a), we assume that the DS can grow with an accretion rate of $\sim 1\,\mathrm{M}_\odot$ to the point where it consumes a significant fraction of the baryons in the halo. In other words, we assume that a $10^7\,\mathrm{M}_\odot$ SMDS will form in a (1–2) $\times\ 10^8\,\mathrm{M}_\odot$ minihalo. While this is an unlikely scenario, which involves most of the baryons in the halo being accreted into a single central object, we will see that even with this assumption, detection rates of SMDS with *JWST* are fairly small. The formation rates in scenario I are plotted in Fig. 2.

As a check, we also broadened the range of DM halo masses in which DS form by allowing halo masses to span a factor of 5 in mass. Fig. 3 (left-hand panel) shows the formation rate $\mathrm{d}n/\mathrm{d}t$ as a function of redshift for haloes in the mass range (1–5) $\times\ 10^7\,\mathrm{M}_\odot$ and the right-hand panel indicates the formation rate of haloes in the mass range (1–5) $\times\ 10^8\,\mathrm{M}_\odot$. In this scenario, the SMDS is 10–50 times smaller than its host halo, and is more realistic since in this case all the baryons in the halo are not accreted by the DS.

A comparison of Figs 2 and 3 shows that the formation rate of host haloes does not vary significantly between the two scenarios (at most by a factor of 3). Henceforth, in the remainder of this study, we will always take the halo mass range to span a factor of 2 in mass.

We define $z_{\rm start}$ to be the (approximate) formation redshift of minihaloes capable of hosting DS, allowing for an uncertainty of a unit redshift interval, i.e. the minimum redshift of minihalo formation is $z_{\rm min} = z_{\rm start} - 1/2$, while the maximum redshift is $z_{\rm max} = z_{\rm start} + 1/2$. We make a distinction between $z_{\rm start}$, the redshift of formation of the DM halo capable of hosting a DS (initial $\sim 1\,\mathrm{M}_\odot$ mini DSs come into existence very soon after this redshift), and $z_{\rm form}$, the redshift of formation of the SMDS. Between $z_{\rm start}$ and $z_{\rm form}$, the DS grows by accreting baryons at a rate of 10^{-2}–$10^{-1}\,\mathrm{M}_\odot\,\mathrm{yr}^{-1}$, growing over this period to a supermassive size of $\sim 10^5$–$10^7\,\mathrm{M}_\odot$. This difference between $z_{\rm start}$ and $z_{\rm form}$ is crucial to accounting for the differences between the results presented in this paper and previous work (Zackrisson et al. 2010b) where this additional time required to grow supermassive was not allowed for.

The formation rate of minihaloes per unit redshift and arcmin^2 is then given by

$$\frac{\mathrm{d}N}{\mathrm{d}z\mathrm{d}\theta^2} = \frac{\mathrm{d}n}{\mathrm{d}t}\left[V_{\rm c}(z_{\rm min}) - V_{\rm c}(z_{\rm max})\right]\frac{C}{4\pi}\Delta t(\mathrm{min};\mathrm{max}), \tag{4}$$

where $V_{\rm c}$ denotes the comoving volume at a given redshift, C is the conversion factor between arcmin^2 and steradians, and Δt(min; max) is the cosmic time interval between $z_{\rm min}$ and $z_{\rm max}$:

$$\Delta t(\mathrm{min};\mathrm{max}) = t_{\rm H}\int_{z_{\rm min}}^{z_{\rm max}} \frac{1}{(1+z)\left[\Omega_{\rm m}(1+z)^3 + \Omega_\Lambda\right]^{1/2}}. \tag{5}$$

The N-body simulations from which the halo formation rates are computed as well as other calculations assume a standard Λ cold DM Universe in which $\Omega_{\rm m} = 0.27$ is the cosmic matter density and $\Omega_\Lambda = 0.73$ is the cosmic dark energy density or cosmological constant with parameters from 5-year *Wilkinson Microwave Anisotropy Probe* (*WMAP*5) data (Komatsu et al. 2009).

We consider three possible redshifts $z_{\rm form}$ by which the DS has accreted enough baryons to become supermassive:

(i) case A: $z_{\rm form} = 10$,
(ii) case B: $z_{\rm form} = 12$,
(iii) case C: $z_{\rm form} = 15$.

In principle, the accretion rate and the final mass of the SMDS in these three cases will imply three different values of $z_{\rm start}$ at which the relevant minihaloes formed. To simplify the situation, we assume a fixed accretion rate of $10^{-1}\,\mathrm{M}_\odot\,\mathrm{yr}^{-1}$ to determine the values for $z_{\rm start}$ (Table 1, column 5), and using corresponding $\mathrm{d}n/\mathrm{d}t$ values from Fig. 2 (Table 1, column 6) at $z = z_{\rm start}$, we evaluate $\mathrm{d}N/\mathrm{d}z\mathrm{d}\theta^2$ using equation (4) (Table 1, column 7). These values of $\mathrm{d}N/\mathrm{d}z\mathrm{d}\theta^2$ will be used in sections to follow.

4 SUPERMASSIVE DARK STARS WITH *Hubble Space Telescope*

In this section, we examine the observability of DSs with existing *HST* surveys, speculating that *HST* may already have seen such objects, if they survive to redshift $z = 10$. We will adopt the standard 'dropout technique' pioneered by Steidel et al. (1996) and applied recently to *J*- and *H*-band observations of the *Hubble Ultra Deep Field* (HUDF09) by Bouwens et al. (2011) and Oesch et al. (2011) to detect a candidate galaxy at $z = 10$ as a '*J*-band dropout'. This photometric redshift determination method requires a 5σ detection of an object in one band but a non-detection in a adjacent band of lower wavelength. In the case of the '*J*-band dropout' observed with *HST*, the object was observed in the 1.60 μm (*H* band) but was *not* seen in the 1.15 μm (*Y* band) or 1.25 μm (*J* band). The absence of emission in the latter bands is assumed to occur due to Lyα absorption by hydrogen clouds in between the source and us, allowing for an approximate estimate of the redshift of the object. More specifically, we take as our dropout criterion

$$\Delta m_{\rm AB} \geq 1.2, \tag{6}$$

where $\Delta m_{\rm AB}$ is the difference in apparent magnitude between the two bands of observation, in this case the *J* and *H* bands. Observations at longer (near to mid-IR) wavelengths are required for photometric determination of objects more distant than $z = 10$, necessitating *JWST* observations. Bouwens et al. (2011) and Oesch et al. (2011) find a candidate $z \sim 10$ object in the co-added first and second year observation of the HUDF with the new WFC3/IR camera as a *J*-band dropout. This object is currently thought to be a galaxy, the most distant one observed to date, since the spectral energy distribution (SED) is a reasonable match to that of galaxies at $z > 9$ and it appears clearly extended (Oesch et al. 2011). Even though it may be hard to identify a DS uniquely with *HST*, the fact that at most one candidate has been found can be used to place bounds on the numbers of DSs at redshifts up to $z = 10$. In this section, we examine the observability of DS of various masses in existing *HST* imaging surveys, and in a later section examine the resulting bounds for future surveys with *JWST*.

4.1 Comparison of DS stellar output with *HST* sensitivity

Figs 4–6 plot the predicted apparent magnitudes of DSs of 10^4–$10^7\,\mathrm{M}_\odot$ at various redshifts and compare these predictions to sensitivity of various *HST* surveys (plotted as thin horizontal lines) in two *HST* filters WFC3 *F*125 (*J* band, coloured blue) and *F*160 (*H* band, coloured red). In these figures, we have assumed that the SMDS formed at $z = 15$ and survived to various redshifts as shown. In Figs 4 and 5, the DSs are considered to be formed via the extended AC mechanism, without any captured DM, while in Fig. 6 we consider the case with capture.

The thick solid curves show the apparent magnitudes $M_{\rm AB}$ for DSs of various masses as a function of redshift in the J_{125} (*F*125*W*, blue) and H_{160} (*F*160*W*, red). These solid curves

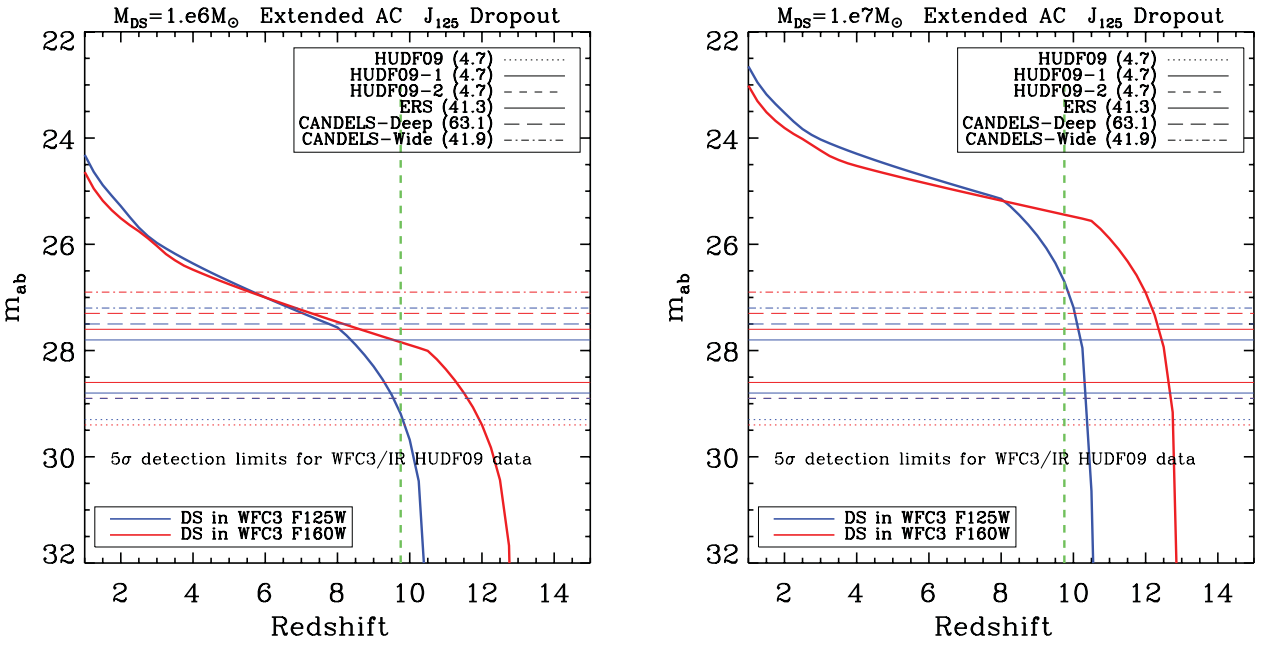

Figure 4. SMDS in *HST*. Left-hand (right-hand) panels: thick curves show apparent magnitudes in the *H* band (*F*160*W*, solid red) and *J* band (*F*125*W*, blue curves) for the $10^6\,M_\odot$ ($10^7\,M_\odot$) versus the redshift of observation for DS formed via extended AC in a $10^7\,M_\odot$ ($10^8\,M_\odot$) halo at redshift of 15. Thin horizontal lines indicate the 5σ detection limits of the various deep field surveys compiled by Oesch et al. (2011), with the areas of the surveys in arcmin^2 indicated in the legends. The deepest survey to date is HUDF09 (lowest dotted horizontal lines). The vertical dashed line is placed at the minimum redshift where the *J*-band dropout criterion is satisfied ($z \sim 10$).

are generated using simulated atmospheres spectra from TLUSTY (Fig. 1) and redshifting them, ($F_\nu(\lambda; z)$), imposing a cut-off at wavelengths lower than the Lyα if $z \gtrsim 6$, assuming that photons at those wavelengths will be absorbed by the neutral hydrogen in the intergalactic medium (IGM). We use the *H* and *J* passbands throughput curves ($T^{H,J}(\lambda)$) for the *HST* WFC3, found at http://www.stsci.edu/~WFC3/UVIS/SystemThroughput/, to compute the observed apparent magnitudes:

$$m_{\rm AB}^{J,H} = -2.5 \log \left[\frac{\int {\rm d}\lambda \lambda T^{H,J}(\lambda) F_\nu(\lambda; z)}{\int {\rm d}\lambda \lambda T^{H,J}(\lambda)} \right] + 31.4. \quad (7)$$

The constant 31.4 is necessary to convert the fluxes to units of nJy. $F(\lambda; z)$ is defined by

$$F_\nu(\lambda; z) = \frac{(1+z) L_{\nu'}(\lambda')}{4\pi D_{\rm L}^2(z)}, \quad (8)$$

where λ is the redshifted wavelength, i.e. $\lambda = (1+z)\lambda'$ and $L_{\nu'}(\lambda')$ is the emitted flux (we use TLUSTY to estimate it). The luminosity distance is labelled by $D_{\rm L}(z)$ and depends on the chosen cosmology. We define a *J*-band dropout to be any observation to the right of the green vertical line, corresponding to a difference in apparent magnitudes of 1.2 or larger between the *J* and *H* filters as defined in equation (6) (the same criterion as used by Oesch et al. 2011). The location of the green line shows that *J*-band dropout technique will also identify the redshift of any SMDS found in this way to be at $z \sim 10$.

In Fig. 4, the sensitivity limits from various deep field surveys compiled by Oesch et al. (2011) – HUDF09, HUDF09-1, HUDF09-2, Early Release Science (ERS) data, CANDELS-Deep and CANDELS-Wide – are indicated by different line styles in the legends on the top right of each panel; these data are compared to the SMDS case of extended AC (no capture). Also shown are the sensitivity limits for various deep field surveys complied in Oesch et al. (2011). *Note also that CANDELS (Grogin et al. 2011; Koekemoer et al. 2011) covers a total of five fields, aimed at mitigating cosmic variance, and that the HUDF and ERS fields are located at one of the CANDELS fields (namely GOODS-S).* In Fig. 5, we focus on the most sensitive of these surveys, HUDF09.[2]

Similarly, Fig. 6 plots the apparent magnitudes as a function of redshift for $10^6\,M_\odot$ (left) and $10^7\,M_\odot$ (right) DSs which grew via captured DM (rather than via extended AC). The SMDSs formed with capture are harder to detect: since they are hotter, their peak output is at lower wavelengths (where Lyα absorption is worse); in addition, their radii are five to 10 times smaller, thus lowering their bolometric luminosities (Freese et al. 2010a). In all cases, the vertical dashed line is placed at the minimum redshift where the *J*-band dropout criterion is satisfied.

For SMDS with masses $\leq 10^5\,M_\odot$, the predicted fluxes in both the *F*125*W* and *F*160*W* filters are too low to be seen in *HST* data; the only way around this would be if the object happened to be gravitationally lensed, as discussed in Zackrisson et al. (2010a). The $10^6\,M_\odot$ DSs can be seen in the *F*125 (*F*160) passbands out to redshifts of 9 (11.5), while the $10^7\,M_\odot$ DS would be detectable out to redshifts of 10.5 (13). However, $10^7\,M_\odot$ DSs would be too bright to be compatible with *HST* data: they would be several magnitudes brighter than the *HST* sensitivity, whereas the observed object is just bright enough to be seen. Thus, the observed $z = 10$ candidate in *HST* cannot be a $10^7\,M_\odot$ DS. In addition, if $10^7\,M_\odot$ SMDS formed at higher redshifts, we can place strong bounds on the numbers of them that can survive down to $z = 10$, where they are not found.

We also note that any SMDS that continued to exist to $z = 6$ would have been seen as an i_{775} dropout in HUDF which has a 29.9 $m_{\rm AB}$ detection limit for 10σ detection in the i_{775} passband (Bouwens

[2] HUDF09 has a limiting 5σ $m_{\rm AB}$ of 29.3 in the *J* band for an exposure time of 94 500 s and 29.4 in the *H* band for an exposure time of 146 711 s for the H_{160} band.

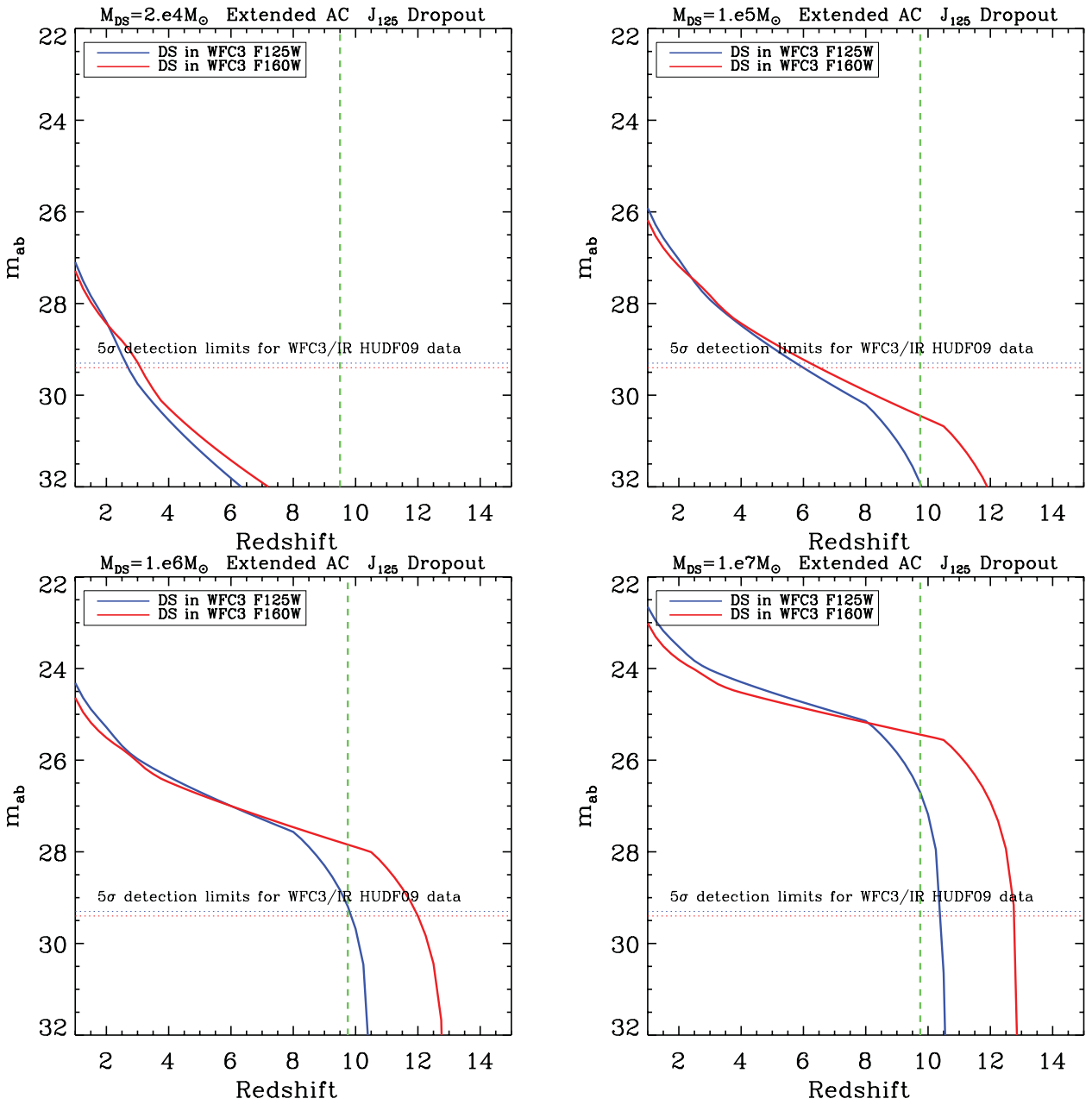

Figure 5. SMDS in *HST*: J_{125} (blue, $F125W$) and H_{160} (red, $F160W$)) apparent magnitudes $M_{\rm AB}$ for DSs of mass ranging between $\sim 10^4$ and $10^7\,{\rm M}_\odot$ as a function of redshift for WFC3 filters. Here the DSs are considered to be formed via the extended AC mechanism, without any captured DM. The dashed horizontal lines represent the sensitivity limits for the deepest survey available, HUDF09. For the H band, the 5σ depth is 29.4, whereas for the J band it is 29.3. The exposure times are $\sim 9.45 \times 10^4$ s for the J_{125} field and $\sim 1.47 \times 10^5$ s for the H_{160} field. The green vertical line corresponds to the lowest redshift where the dropout criterion is satisfied. Compared to Fig. 4 now we explore a wider mass range for the SMDS. Note that SMDS of mass $10^5\,{\rm M}_\odot$ or lower cannot be observed as J-band dropouts with current *HST* data (another factor of 100 in observing time would be required), whereas heavier SMDS can be detected.

et al. 2006). Since no candidates exist in the data, this makes it clear that SMDS did not survive to $z = 6$. Thus, we conclude that it is the $10^6\,{\rm M}_\odot$ SMDS that serves as the best possible explanation for the J-band dropout at $z = 10$ seen by *HST*.

4.2 Using *HST* observations to constrain the numbers of dark stars

We will use *HST* data to constrain the fraction $f_{\rm SMDS(z_{start})}$ of early DM haloes that can host SMDS. We focus on SMDS of masses $M_{\rm DS} = 10^6$–$10^7\,{\rm M}_\odot$ since lower mass DSs are not observable in current *HST* data (unless they are significantly magnified by gravitational sensing or if they form clusters of DSs; Zackrisson et al. 2010b).

Following Zackrisson et al. (2010b, 2011b), we compute the number $N_{\rm obs}$ of DS that could potentially be observed,

$$N_{\rm obs} = \frac{{\rm d}N}{{\rm d}z{\rm d}\theta^2} f_{\rm SMDS}(z = z_{\rm start})\theta^2 f_{\rm surv} f_{\Delta t}, \quad (9)$$

and use the fact that at most one object has been observed with *HST* at $z = 10$ to obtain bounds on $f_{\rm SMDS(z_{start})}$, the fraction of DM haloes

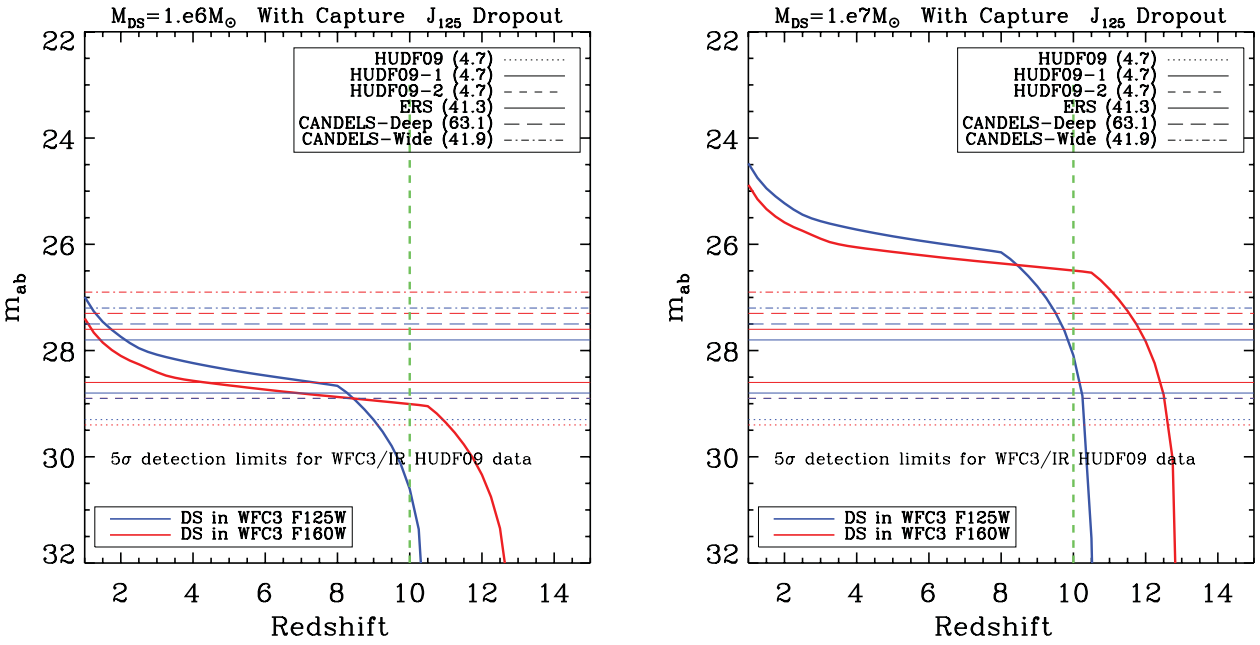

Figure 6. SMDS in *HST*: same as Fig. 5 but for 10^6–10^7 $M_\odot$ DSs fuelled by captured DM. The dashed horizontal lines represent the sensitivity limits for the deepest survey available, HUDF09.

in a given mass range that can host a DS:

$$N_{\rm obs}^{\rm HST} < 1. \quad (10)$$

Here $dN/dz d\theta^2$ is the number of DM haloes forming per unit redshift per arcmin^2 in which a given mass DS is hosted (computed from Fig. 2). We have multiplied by unit redshift interval $\Delta z = 1$, since we only consider SMDS formed within a redshift interval equal to 1 (see the discussion following equation 1). Here θ^2 is the total area surveyed in which the SMDS could have been detected, $f_{\rm surv}$ is the fraction of DS that survives from the redshift where the DS starts forming, $z_{\rm start}$, until it could be observed as a dropout (at $z \sim 10$ with *HST*) and $f_{\Delta t}$ is the fraction of the observational window of time Δt during which the DS is still alive. Here, Δt is the cosmic time elapsed between the minimum and maximum redshift where the DS could be observed as a dropout. Please note that those redshifts are different from $z_{\rm min}$ and $z_{\rm max}$ defined under equation (4). For the case of *HST*, we get $\Delta t = 6.5 \times 10^7$ yr (the cosmic time between the minimum redshift of 9.5 and maximum redshift of 10.5 where the DS could be observed as a *J*-band dropout computed using equation 5).

We estimate the survey area θ^2 in the following way. For each of the surveys in Figs 4 and 6, we have indicated (in parentheses in the plots) the area (in arcmin^2) observed by the survey. For DS of a given mass, we can add up the areas of all those surveys which are capable of observing DS as *J*-band dropouts to obtain a total effective area of observability for that DS mass. In other words, we add the area of all surveys in which the fluxes in the H_{160} are still above the sensitivity limits, while the fluxes in the J_{125} are a least 1.2 lower in apparent magnitude and below the detection limit of the *J* band. From Fig. 4, we estimate $\theta^2 = 4.7 \times 3$ arcmin^2 as the effective area of the surveys in which a 10^6 $M_\odot$ SMDS formed via extended AC could have been observed as a *J*-band dropout with *HST*, since it is only for the three deepest surveys, each with an area of 4.7 arcmin^2, that this SMDS would show up as a dropout. For the 10^6 $M_\odot$ SMDS formed via captured DM, the detectability is much lower, implying that they could have been observed with *HST* WFC3 as a *J*-band dropout only in the deepest survey, namely in HUDF09, which has an area of 4.7 arcmin^2.

Although the $z = 10$ *J*-band dropout seen by *HST* cannot be a 10^7 $M_\odot$ SMDS (as it would be too bright and would show up in both bands), still we can apply equation (9) to place an upper bound on the numbers of these objects. For the 10^7 $M_\odot$ stars formed via extended AC, this area is increased to $\sim$160 arcmin^2, as all surveys compiled could pick this object up as a *J*-band dropout. For the hotter DS fuelled by captured DM, we can see from Fig. 6 that the total area of the surveys in which 10^7 $M_\odot$ DS could have been detected is $\sim$160 arcmin^2 (similar with the area for the extended AC DS of the same mass).

We comment here on the three redshifts of formation we have chosen. For a conversion between $z_{\rm form}$ (redshift where the DS reaches its final mass) and $z_{\rm start}$ (the redshift where the DS starts accreting baryons), see Table 1.

(i) *Case A:* $z_{\rm form} = 10$. Here, we assume that the DS becomes supermassive only at $z = 10$ and not before. We can only constrain the product $f_{\rm SMDS} \times f_{\rm surv} \times f_{\Delta t}$. The fraction of the observational window during which the DS is alive and can be observed is $f_{\Delta t} = \min(\tau - \tau_{\rm min}, \Delta t)/\Delta t$, where $\tau_{\rm min}$ is the minimum DS lifetime that allows the DS to survive to $z = 10.5$ where it can be observed as a *J*-band dropout with *HST*. In the case of a 10^7 $M_\odot$ SMDS, $\tau_{\rm min} \sim 1.15 \times 10^8$ yr (time elapsed between $z = 13$ and 10.5), whereas for the 10^6 $M_\odot$ SMDS $\tau_{\rm min} \sim 3.6 \times 10^7$ yr (cosmic time elapsed between $z = 10.7$ and 10.5). We note that the limits we place on $f_{\rm SMDS}(z_{\rm start})$ are only valid at $z_{\rm start} \sim$13 (for the 10^7 $M_\odot$ SMDS) and $z_{\rm start} \sim$11 (for the 10^6 $M_\odot$ SMDS) as can be seen from Table 1.

(ii) *Case B:* $z_{\rm form} = 12$. Here we consider the DS to become supermassive at $z_{\rm form} \sim$12 and not at later redshifts. We will assume that the DS could survive until $z \sim 10$ ($f_{\rm surv} = 1$) in order to constrain $f_{\rm SMDS}(z_{\rm start})$ using null detection from *HST* J_{125} dropouts. From Table 1, we see that the $z_{\rm start}$ value for the 10^7 $M_\odot$ SMDS in this case is $\sim$16 and for the 10^6 $M_\odot$ SMDS it is $\sim$13. In the case of a 10^7 $M_\odot$ SMDS, $\tau_{\rm min} \sim 2.0 \times 10^8$ yr, whereas for the 10^6 $M_\odot$ SMDS $\tau_{\rm min} \sim 1.1 \times 10^8$ yr.

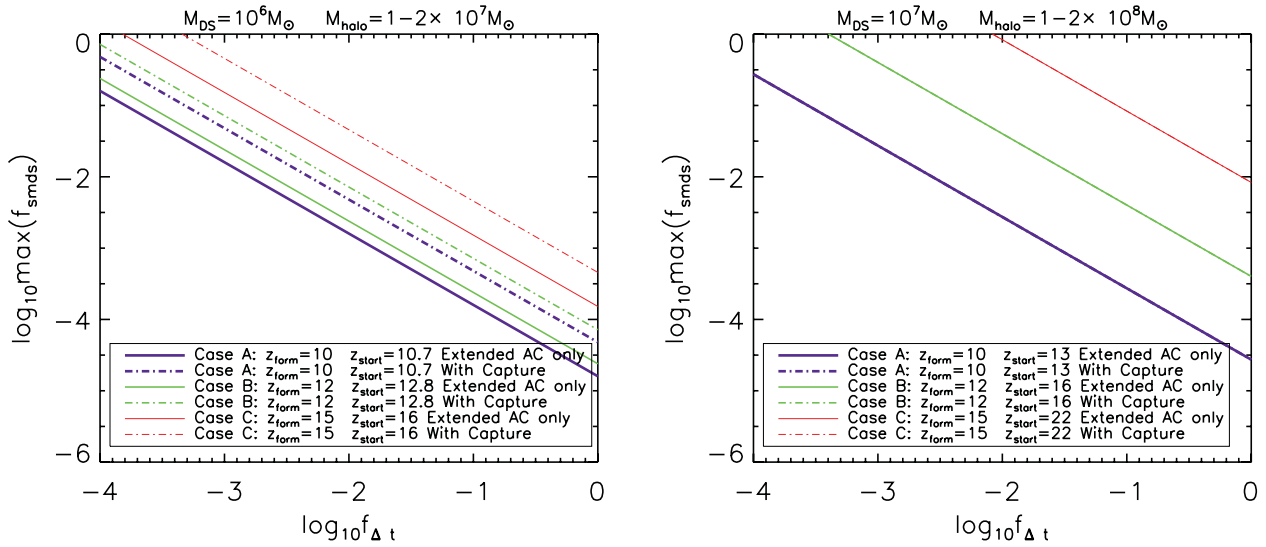

Figure 7. Upper bounds from *HST* on the fraction $f_{\rm SMDS}$ of early halo hosting DSs of masses as labelled above the plots; values above the lines are excluded. Different lines correspond to different values of the redshift ($z_{\rm form} = 10$, 12 and 15) at which the DS attains this mass; see Table 1 for the connection between (a) the redshift $z_{\rm start}$ at which the DS came into existence and started to grow and (b) the redshift $z_{\rm form}$ at which it reached the supermassive size as labelled. This plot assumes $f_{\rm surv} = 1$ (i.e. the DS survives long enough to reach the redshift window of observability as a J_{125} dropout with *HST*). However, the DS need not survive throughout the entire window; in fact, the horizontal axis in both plots is $\log_{10} f_{\Delta t}$, for which a value of 0 corresponds to the DS lifetime being sufficiently large that it survives throughout the redshift window of observability. Solid lines correspond to DS formation via extended AC (without capture), while dashed lines correspond to DS formation via capture. Since DS less massive than $10^6\,{\rm M}_\odot$ are too faint to be detected by *HST*, these data do not bound $f_{\rm SMDS}$ for lower mass DSs.

(iii) *Case C:* $z_{\rm form} = 15$. Here we assume the DSs become supermassive by $z_{\rm form} \sim 15$. The values for $z_{\rm start}$ can be read off from Table 1 again. For the $10^7\,{\rm M}_\odot$ SMDS $z_{\rm start} \sim 22$ and for the $10^6\,{\rm M}_\odot$ SMDS $z_{\rm start} \sim 16$. This case is treated in a similar fashion as case B. For the $10^7\,{\rm M}_\odot$ SMDS, $\tau_{\rm min} = 2.9 \times 10^8$ yr (the time elapsed between redshifts 22 and 10.5), whereas for the $10^6\,{\rm M}_\odot$ SMDS $\tau_{\rm min} = 2.0 \times 10^8$ yr (the time elapsed between redshifts 16 and 10.5).

From equation (9), we obtain the following bounds for $10^7\,{\rm M}_\odot$ SMDS formed via either extended AC or with capture in each of the three cases (A–C):

$$\log f_{\rm SMDS}\left(M_{\rm DS} = 10^7\,{\rm M}_\odot\right) \leq \begin{cases} -4.5 - \log(f_{\rm surv} \times f_{\Delta t}), & {\rm A} \\ -3.4 - \log(f_{\rm surv} \times f_{\Delta t}), & {\rm B} \\ -2.1 - \log(f_{\rm surv} \times f_{\Delta t}), & {\rm C}. \end{cases} \quad (11)$$

For $10^6\,{\rm M}_\odot$ SMDS formed via extended AC, we get the following limits:

$$\log f_{\rm SMDS}\left(M_{\rm DS} = 10^6\,{\rm M}_\odot\right) \leq \begin{cases} -4.8 - \log(f_{\rm surv} \times f_{\Delta t}), & {\rm A} \\ -4.6 - \log(f_{\rm surv} \times f_{\Delta t}), & {\rm B} \\ -3.8 - \log(f_{\rm surv} \times f_{\Delta t}), & {\rm C}. \end{cases} \quad (12)$$

The values of $z_{\rm start}$ that correspond to these values of $z_{\rm form}$ can be found in the last three rows of Table 1. The reason that the bounds on the numbers of $10^6\,{\rm M}_\odot$ SMDS are tighter than those on the $10^7\,{\rm M}_\odot$ SMDS is the following. In order to reach a larger mass, the DS had to start forming at an earlier redshift and in larger haloes; but the numbers of larger haloes that can host DS are smaller at higher redshifts. Similarly, the bounds in case A are $\sim$10 ($\sim$300) times stronger than the bounds in case C for the $10^6\,{\rm M}_\odot$ ($10^7\,{\rm M}_\odot$) SMDS. Again the reason for the very large discrepancy ($\sim$300) is the fast decrease of the formation rate of 1–2 $\times 10^8\,{\rm M}_\odot$ DM haloes at redshifts higher than $z \sim 15$ as can be seen from Fig. 2. For SMDS lighter than $10^6\,{\rm M}_\odot$, *HST* cannot be used to place constraints, as those objects are not detectable with *HST* as *J*-band dropouts. A summary of our bounds can be found in Fig. 7, where we plot the exclusion limits for $f_{\rm SMDS}$.

4.3 Other bounds on numbers of SMDS

Further bounds on the numbers of DS and the haloes they form in should result from a variety of considerations. One would be the contribution to reionization. Work of Venkatesan (2000) studied stellar reionization with the standard fusion-powered first stars (Pop III), without any DSs. From comparison with the optical depth to last scattering from early *WMAP* data, she bounded the fraction of baryons in haloes that can cool and form stars (assuming a Scalo IMF) to be in the range $f_* \sim 0.01$–0.1. However, it is not clear how these numbers would change in the presence of DS and with the updated value for the optical depth from *WMAP*7 (Komatsu et al. 2011).

More recently, the effects of DS (and the resultant main-sequence stars) on reionization were studied by Schleicher et al. (2008, 2009) and Scott et al. (2011). While DS are fully DM powered, they remain so puffy and cool that no ionizing photons are produced, and there is no contribution to reionization. However, once the DM fuel begins to run out, they contract and heat up as they approach the zero-age main sequence (ZAMS) with the onset of fusion, at which point they do produce ionizing photons. For the case of extended AC, and for DS less massive than $1000\,{\rm M}_\odot$, Scott et al. (2011) concluded that the reionization history of the Universe is unaffected by the DS, compared to the case of more standard Pop III stars: the DS period of no ionizing photon production is compensated by a short period of high-ionizing photon production during approach to the ZAMS. However, we are not sure what the effect on reionization would be

in the case of the more massive SMDS. On the one hand, the more massive stars are hotter and brighter and would emit substantial amounts of ionizing photons; on the other hand, the more massive the star, the shorter the lifetime.

For the case of DS with high capture rates, previous studies (Scott et al. 2011) find that reionization is somewhat delayed, decreasing the integrated optical depth to the surface of last scattering of the cosmic microwave background. However, variation of astrophysical parameters for the case of standard reionization with standard Pop III stars can produce exactly the same effect, so that disentangling these effects will prove difficult. Nonetheless, Scott et al. (2011) do argue that they can rule out the section of parameter space where DSs $\sim$1000 $M_\odot$ with high scattering-induced capture rates tie up more than 90 per cent of all the first star-forming baryons and live for more than 250 Myr. Again, their work should be extended to the heavier SMDS we study in this paper.

First, a complicating factor (for both the cases of extended AC and capture) is that the SMDS do eventually collapse to BH, and it is not clear how rapidly that happens. If the collapse to BH is rapid, this may cut short the ZAMS phase and reduce the role SMDSs play in reionization. Secondly, the SMDSs are likely to have stellar pulsations (Montgomery et al., in preparation); as a consequence, it is possible they will lose some mass before reaching the ZAMS. Thirdly, even after joining the ZAMS, en route to BH collapse, the SMDS may blow off some of their mass [Umeda et al. (2009) suggest 1/2 of their mass].

Heger (private communication) has the following new results for early stars (only made of hydrogen and helium) that are non-rotating: if they are heavier than 153 000 $M_\odot$, no hydrostatic equilibrium solution exists, i.e. no primordial hydrogen burning star exists. Thus, once a fusion-powered star accretes enough mass to get heavier than this, then it collapses straight to a BH. For any of our DSs that are heavier than this, once they run out of DM, they collapse directly to BH without contributing at all to reionization. Rotation might change these results.

Further, there are implications of DS regarding the fraction of baryons that end up in DSs. Our work assumes that the DS can grow in a DM halo of a given mass until almost all the baryons in the halo (assumed to be the baryonic mass fraction in the Universe) are accreted on to the DS. If the total fraction of haloes in which such DSs form is too large, this implies that most of the baryons in the Universe are trapped inside DS and it is not clear how they would contribute any further to galaxy formation. As mentioned above, en route to BH collapse, the SMDS may blow off some of their mass, reinjecting baryons into the surrounding haloes and alleviating this problem somewhat.

Further bounds on the numbers of DSs have been studied in Sandick et al. (2011). The remnant BHs from the DS should still exist today, including inside the Milky Way. They still have enhanced amounts of DM around them, known as DM spikes. The DM inside the spikes annihilates to a variety of final products, with γ-rays that would be detected by the *Fermi Gamma Ray Space Telescope* (*FGST*). In Sandick et al. (2011), it was noted that most of the 368 point sources observed by *FGST* might in fact be due to DM annihilation in the spikes. In addition, *FGST* data were used to place bounds on the fraction of early haloes hosting DS to avoid overproduction of γ-rays from annihilation in the remnant DM spikes. The bounds range from $f_{\rm DS} < 10^{-3}$–1, depending on the WIMP mass and annihilation channel.

All of these considerations are beyond the scope of this paper. For now, we take these arguments to imply that not every early halo can contain a DS.

Table 2. 10σ sensitivity limits for the *JWST* wide passband filters (fourth column). The $m_{\rm AB}$ limits are derived assuming 10^4-s exposure and are based on the limiting fluxes published at http://www.stsci.edu/jwst/instruments/miri/sensitivity/ and http://www.stsci.edu/jwst/instruments/nircam/sensitivity/table*. We identify each filter by its name, in the first column. Values in the second column correspond to the centre wavelength of each filter, whereas in the fourth column the values for the passband width are given.

	Filter	$\lambda_{\rm centre}$ (μm)	$\log_{10}\lambda_{\rm centre}$	$\Delta\lambda$ (μm)	$m_{\rm AB}$
NIRCam	*F*070*W*	0.7	−0.15	0.175	28.1
	*F*090*W*	0.9	−0.05	0.225	28.51
	*F*115*W*	1.15	0.06	0.2875	28.72
	*F*150*W*	1.5	0.17	0.375	28.77
	*F*200*W*	2.0	0.30	0.5	28.75
	*F*277*W*	2.77	0.44	0.6925	28.67
	*F*356*W*	3.56	0.55	0.89	28.55
	*F*444*W*	4.44	0.65	1.11	27.92
MIRI	*F*560*W*	5.6	0.75	1.2	25.65
	*F*770*W*	7.7	0.89	2.2	25.28
	*F*1000*W*	10.0	1.00	2.0	24.29
	*F*1130*W*	11.3	1.05	0.7	23.32
	*F*1280*W*	12.8	1.1	2.4	23.53
	*F*1500*W*	15.0	1.18	3.0	23.26
	*F*1800*W*	18.0	1.25	3.0	22.31
	*F*2100*W*	21.0	1.32	5.0	21.56
	*F*2550*W*	25.5	1.4	4.0	20.28

5 OBSERVING SUPERMASSIVE DARK STARS WITH *JWST*

DSs can be detected by upcoming *JWST*. Table 2 gives a summary of the sensitivity of the NIRCam and MIRI cameras on *JWST* in various wavelength bands.[3] One can see that the NIRCam is much more sensitive than the MIRI filters, so that light emitted at wavelengths larger than 5 μm is harder to observe. In this section, we estimate the number of SMDS that would show up in a typical survey with *JWST* NIRCam or MIRI cameras, based on the bounds we have just derived in the previous section.

Figs 8–11 illustrate the detectability of SMDS with *JWST* NIRCam filters. Figs 8 and 9 plot the stellar spectra of SMDSs of various masses and formation redshifts as a function of wavelength (for light emitted at $z = 15$, 10 and 5) and compare to the sensitivity of *JWST* filters for 10^4 and 10^6 s exposure times. In Figs 10 and 11, we instead plot the apparent magnitudes as a function of redshift of emitted light for various SMDS through the NIR camera wide passband filters, with each panel in the figure focusing on a particular *JWST* broad-band filter; in these two figures, the SMDS are formed via extended AC and capture, respectively. Lyα absorption cuts off the photons with wavelengths lower than 1216 Å (in the rest frame); we treat the absorption as being complete. Thus, the SMDSs drop below the *JWST* sensitivity limit at $z \sim 6$ for the *F*070*W* filter and at $z \sim 10$ for the *F*115*W* case.

[3] Specifically, we show the 10σ required $m_{\rm AB}$ sensitivities for the NIRCam and MIRI wide filters after 10^4-s exposure derived based on the limiting fluxes published at http://www.stsci.edu/jwst/instruments/miri/sensitivity/ and http://www.stsci.edu/jwst/instruments/nircam/sensitivity/table*. One can scale the limits to different exposure times, as the limiting flux $\propto t_{\rm exposure}^{-1/2}$ and converting to $m_{\rm AB}$ magnitudes is just a matter of applying equation (7). For instance, an increase by a factor of 100 in exposure times would convert in a gain in the sensitivity limits by 2.5 AB magnitudes.

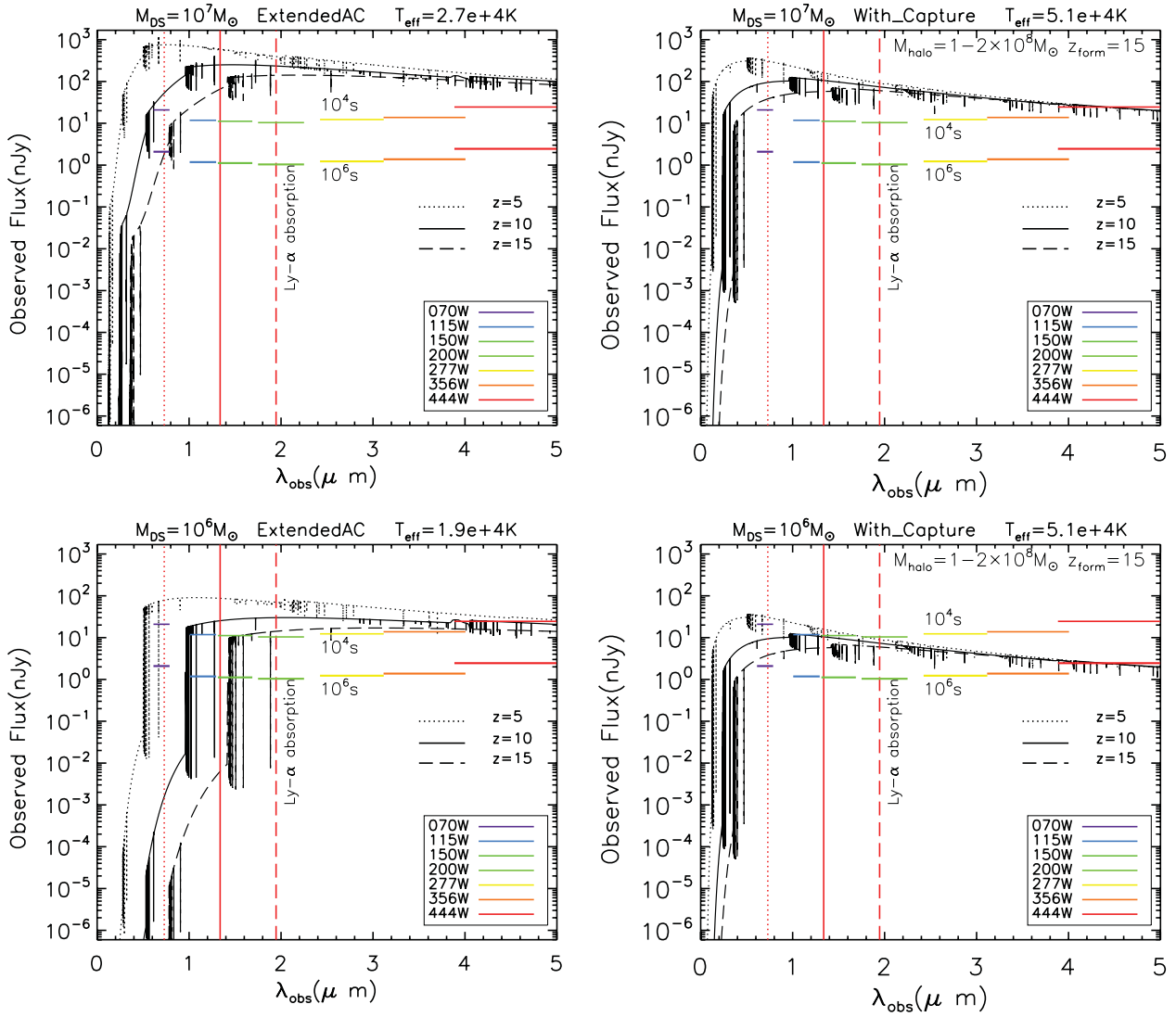

Figure 8. Spectra for SMDS formed at $z_{\rm form} = 15$ compared with sensitivity of *JWST* filters. Listed above each panel are the mass of the DS in solar masses, the formation mechanism (extended AC or 'with capture') and the surface temperature $T_{\rm eff}$. The fluxes are shown at $z = 15$ (dashed line), 10 (solid line) and 5 (dotted line) and compared to the detection limits of NIRCam wide passband filters. The coloured horizontal lines represent the sensitivity limits for the filters as labelled in the legend for exposure times 10^4 s (upper lines) and 10^6 s (lower lines). IGM absorption will decrease the observed fluxes for wavelengths shortwards of the vertical red lines, which indicate the Lyα line (1216 Å) redshifted from the rest frame of the star.

Since the most massive DSs are the brightest, they are the easiest to detect. From Figs 10 and 11, one can see that 10^7 M$_\odot$ DSs, both with and without capture, are individually observable in 10^4 s of NIRCam data even at redshifts as high as 15 in filters with a passband centred at 2 μm and higher (*F*200*W*–*F*444*W* filters). For the case of a 10^6 M$_\odot$ SMDS, a longer exposure time of 10^6 s allows the DS, both with and without capture, to be individually observable in all filters from *F*200*W* to *F*444*W* even at $z \sim 15$. For 10^5 M$_\odot$ SMDS, those formed via extended AC are visible in these filters out to $z \sim 15$ with 10^6 s exposure time, while those formed with capture are too dim. Lighter ones $<10^5$ M$_\odot$ would not be detectable as *J*-band dropouts but, if they survived to lower redshifts (e.g. $z = 7$), they would likely already have been seen with *HST* or other telescopes. Since the sensitivity of the higher wavelength MIRI filters above 5 μm is worse, only the 10^7 M$_\odot$ DS are bright enough to be observable in MIRI filters (see the discussion of Fig. 15 in Section 6).

5.1 Detection at $z \sim 10$ as a J_{115}-band dropout with *JWST*

The DSs that could have been detected as *J*-band dropouts with *HST* are also detectable as dropouts of various types in *JWST*: *J*-, *H*- and *K*-band dropouts, as will be studied in the next three sections. In this section, we focus on *J*-band dropouts, where the object would be detected as being much brighter in the *F*150 NIRCam filter of *JWST* than in the *F*115 NIRCam filter. As before in equation (6), we require the difference between the broad-band fluxes in the J_{115} and H_{150} filters to be greater than 1.2 AB magnitudes. We see that the SMDS stellar light seen with *JWST*'s H_{150} is essentially unaffected by Lyα absorption until $z \gtrsim 11.5$, whereas the IGM absorption will cut off most of the flux in the J_{115} at $z \gtrsim 9.5$ (see Figs 10 and 13). Thus, an SMDS detected as *J*-band dropouts in *JWST* would be identified as having a redshift $z \sim 10$ (in between these two values).

Fig. 12 shows the sensitivity of *JWST* in a 10^4-s exposure in the 1.15 μm (*J* band) and 1.50 μm (*H* band) filters for NIRCam. The

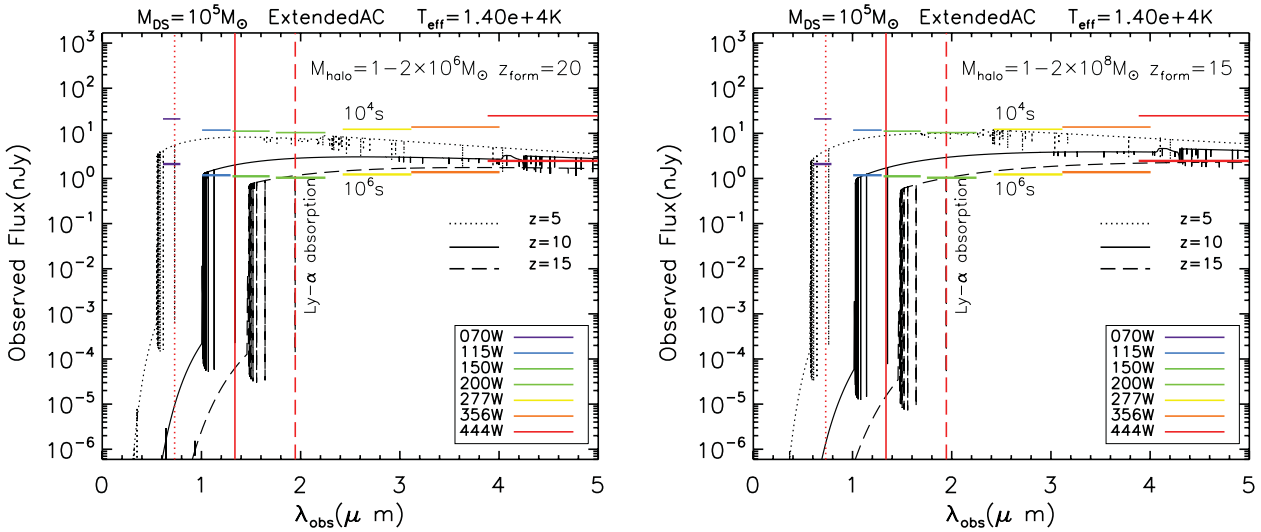

Figure 9. Similar to Fig. 8, now for a 10^5 $M_\odot$ DS formed either at $z_{form} = 20$ in a 10^6 $M_\odot$ DM halo (left-hand panel) or at $z_{form} = 15$ in a 10^8 $M_\odot$ DM halo (right-hand panel).

apparent magnitudes for 10^6 and 10^7 $M_\odot$ SMDS with and without capture are also shown for comparison. Here, the SMDSs form at $z = 15$ and are assumed to survive to various redshifts as shown. Comparing Figs 4 and 12 (see also Table 2), one can see that *JWST* is about half a magnitude more sensitive than *HST* to finding SMDS as *J*-band dropouts (for 10^5 s exposure time with numbers provided in the literature as 5σ detection in HUDF09 and 10σ detection with *JWST*).

The three cases of 10^7 $M_\odot$ with or without capture as well as 10^6 $M_\odot$ without capture could be detectable in a *JWST* survey as *J*-band dropouts in the redshift range 9.5–12 even with the lower 10^4 s exposure times. The 10^6 $M_\odot$ DS formed via captured DM (lower left-hand plot) in Fig. 12 will require a longer exposure time of 10^6 s (which would correspond to the same exposure time as the 2004 HUDF survey).

In order to predict how many SMDS would be visible in a *JWST* deep field survey, we have to assume something about the total field of view (FOV) of all future *JWST* surveys in which the stars would be observable. The FOV of the NIRCam instrument is $2.2 \times 4.4 = 9.68$ arcmin^2 (see http://www.stsci.edu/jwst/overview/design/). This value is likely to be an underestimate. Since *HST* had multiple surveys with a total of 160 arcmin^2, we will also consider the case of multiple field surveys with *JWST* with a total added area of $\sim$150 arcmin^2. Given the bounds on the numbers of DS from *HST* from the previous section, we find that the number of expected SMDS with *JWST* as *J*-band dropouts is $N \lesssim 1$ and therefore conclude that SMDSs are hard to detect with *JWST* as *J*-band dropouts. This is expected since *HST* was already sensitive enough to observe them as *J*-band dropouts, assuming enough would have survived from their formation redshift until $z \sim 10$. The only improvement could be made by a larger survey area compared to the one with *HST*. For the 10^6 $M_\odot$ SMDSs formed with capture, which were detectable only in the 4.7 arcmin^2 of HUDF09, *JWST* should be able to provide a larger survey area so that these objects become more detectable.

5.2 Detection at $z \sim 12$ as a H_{150}-band dropout with *JWST*

Whereas *JWST* is not particularly better than *HST* at finding *J*-band dropouts, it will be significantly better at finding SMDS as *H*- and *K*-band dropouts at higher wavelengths. In this section, we focus on *H*-band dropouts, where the object can be seen in the *F*200 NIRCam filter of *JWST* but not in the *F*150 NIRCam filter. As before in equation (6), we require the difference between the broad-band fluxes in the H_{150} and K_{200} filters to be greater than 1.2 AB magnitudes. We see that the SMDS stellar light seen with *JWST*'s K_{200} filter is essentially unaffected by Lyα absorption until $z \sim 15$, whereas the IGM absorption will cut off most of the flux in the H_{150} at $z \gtrsim 11.5$ (see Fig. 13). Hence, SMDS can appear as *H*-band dropouts.

We will consider the case of SMDS forming at $z_{form} = 12$, the same as the time of observation. Fig. 13 shows that the three cases of 10^7 $M_\odot$ SMDSs with and without capture as well as 10^6 $M_\odot$ SMDSs without capture are all detectable in a *JWST* survey as H_{150} dropouts in the redshift range 11.5–12.5. DS formed at higher redshifts could be seen all the way out to $z \sim 14$ and 15, but likelihood analyses on any objects found as *H*-band dropouts with photometry with *JWST* will probably estimate the redshift at $z \sim 12$. The 10^6 $M_\odot$ DS formed via captured DM (lower left-hand plot) is too faint to appear as a dropout. The number of H_{150} dropout events is given by equation (9) with $\Delta z = 1$ and $f_{surv} = 1$ since the objects are observed at the same time they form and the appropriate survey area θ^2 for *JWST* must be applied.

Is it reasonable to apply the bounds from *HST* on the numbers of SMDS at $z = 10$ to those at $z = 12$? We will consider three different possibilities, and summarize all results for the predicted number of *H*-band dropouts with *JWST* in Table 3. If we assume that all the SMDS at $z = 12$ have the same properties as those at $z = 10$, and that they survive throughout the redshift window observable by *HST*, then the *HST* bounds are so stringent that *JWST* will not be able to see many of them. This is the case we label 'maximal bounds'. In particular, 10^7 $M_\odot$ SMDSs would have been so bright as to be easily seen in *HST*, and the resultant stringent bounds imply that only $N_{obs} \sim 1$ DS would be found even with multiple field surveys with 150 arcmin^2 FOV. For 10^6 $M_\odot$ SMDSs, the bounds from *HST* are slightly weaker because the objects are not as bright, so that 10 (32) of these might be found per 150 arcmin^2 field for DS that grew via extended AC (with capture). Since the ones with capture are fainter and harder to see (counterintuitively), the weaker *HST* bounds imply that more of them might be found with *JWST*.

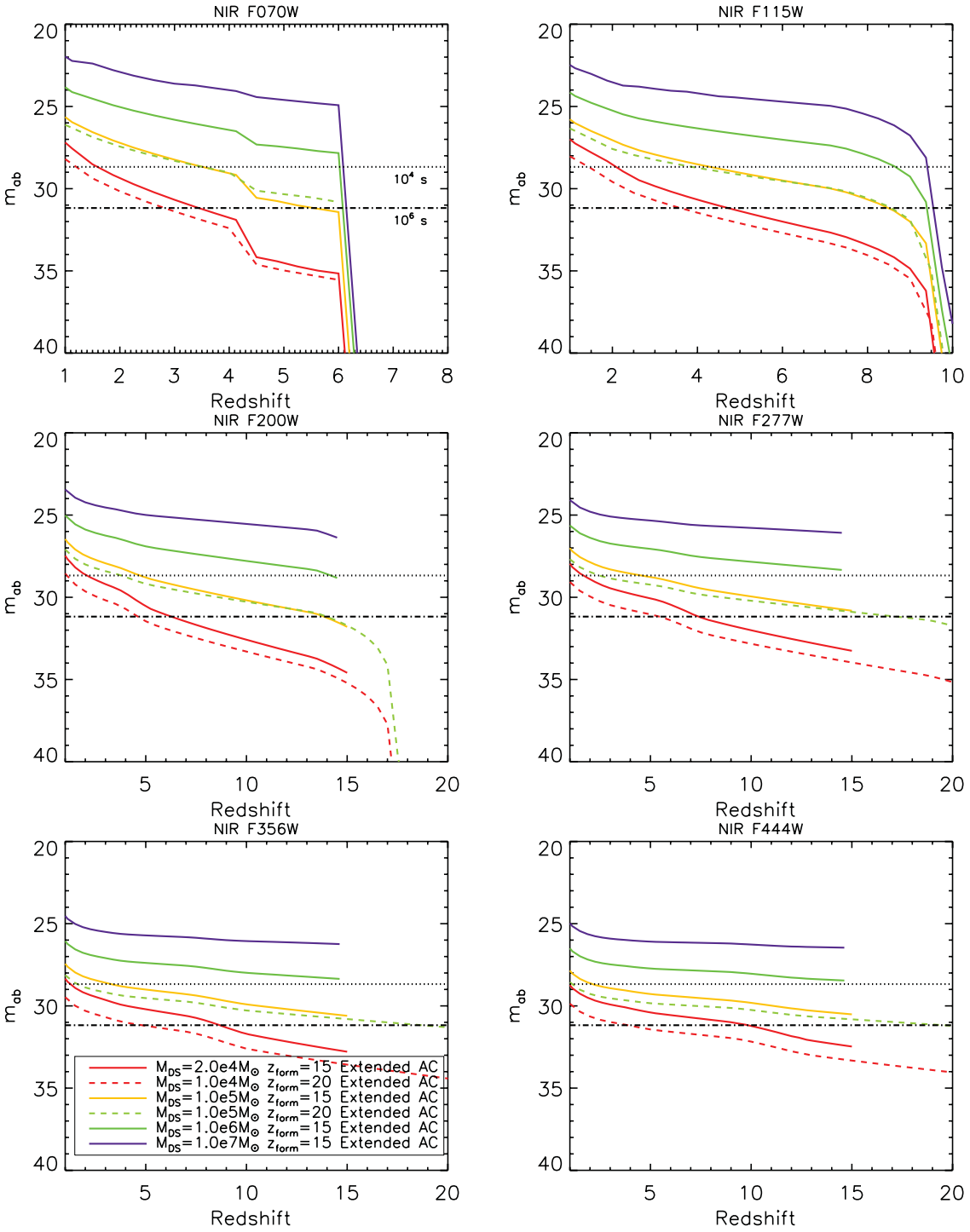

Figure 10. Apparent magnitudes as a function of redshift for various SMDS through the NIR camera wide passband filters on *JWST* for the case of formation via extended AC. The number after the letter F and before the letter W in the name of each filter corresponds to the wavelength in the centre of the passband in 0.01 μm units. The two horizontal lines correspond to sensitivity limits for each filter for 10^4 s exposure time (the dotted line) and 10^6 s exposure time (the dot–dashed line). The $z_{\rm form}$ labelled in the legend is the formation redshift when the SMDS reached its corresponding mass. The curves corresponding to $z_{\rm form} = 15$ do not extend all the way to $z = 20$ because at that high redshift the star has not formed yet. The sharp decrease of the fluxes at various redshifts in the first three panels is due to the Gunn–Peterson trough entering the filters. The higher wavelength filters *F*277*W*–*F*444*W* would not be affected by the IGM absorption until $z \gtrsim 20$.

However, it is very likely that there are more SMDS at $z = 12$ (the *JWST* window) than at $z = 10$ (the *HST* window). For one thing, the host halo formation in this mass range peaks at $z \sim 12$ (see Fig. 3). Moreover, at lower redshifts ($z \sim 10$) the DM haloes that could host those SMDSs are much more likely to merge to form even larger haloes. In addition, after the first SMDSs die (before $z = 10$), they turn into fusion-powered stars that produce ionizing photons, which disrupt the formation of DS at lower redshifts. Indeed, the

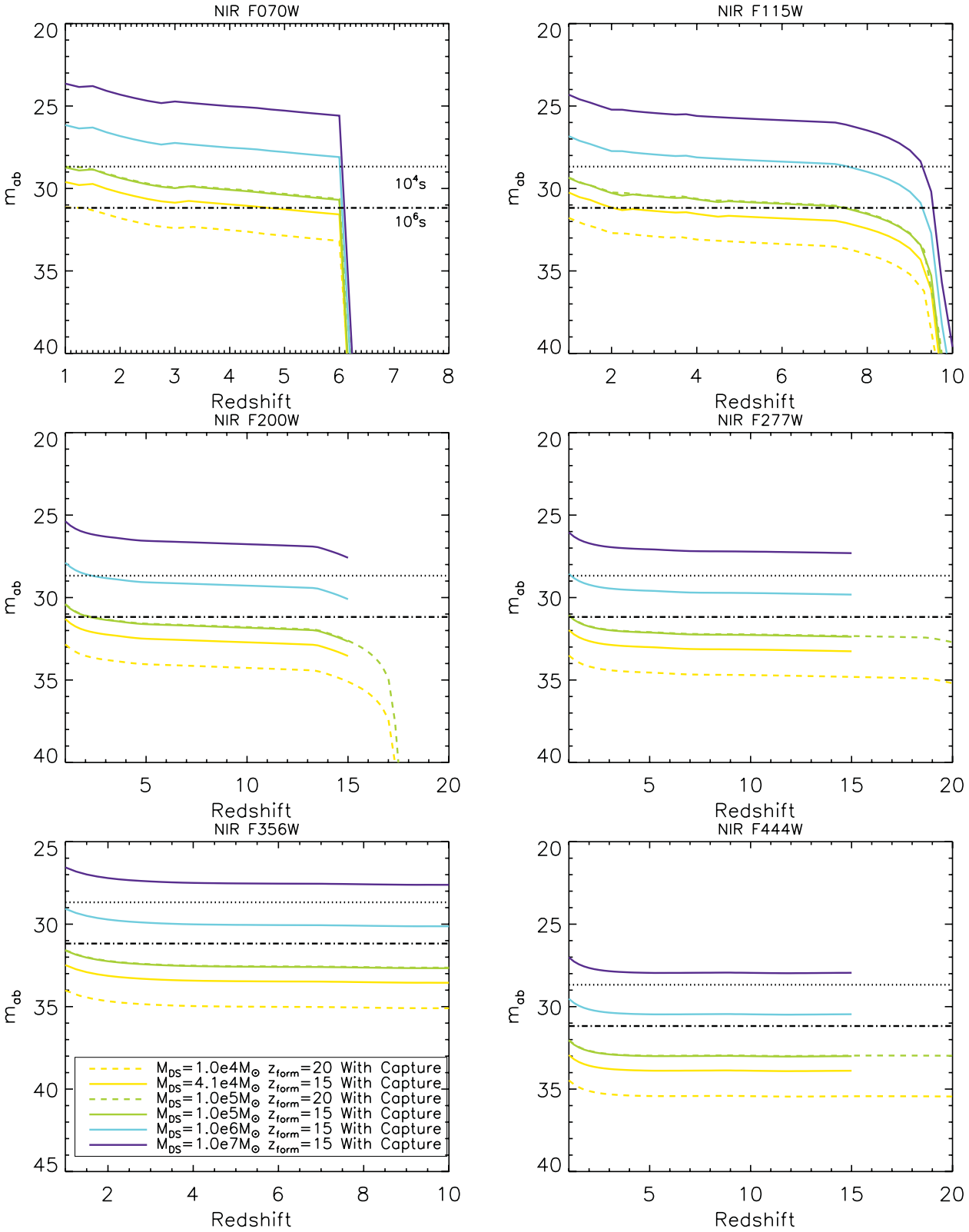

Figure 11. Same as Fig. 10 for SMDS formed 'with capture' in various *JWST* bands as labelled.

strong halo clustering at high redshift would cause the possible formation sites to be preferentially close to or inside the H II regions during reionization, potentially leading to strong suppression of star formation; due to this mechanism, Iliev et al. (2007) found a suppression of 10^8–10^9 $M_\odot$ haloes by an order of magnitude due to Jeans mass filtering in the ionized and heated H II regions.

We will thus recalculate the number of DSs detectable with *JWST* using weakened bounds from *HST*. We will take $f_{\rm SMDS} f_{\Delta t} f_{\rm surv} =$

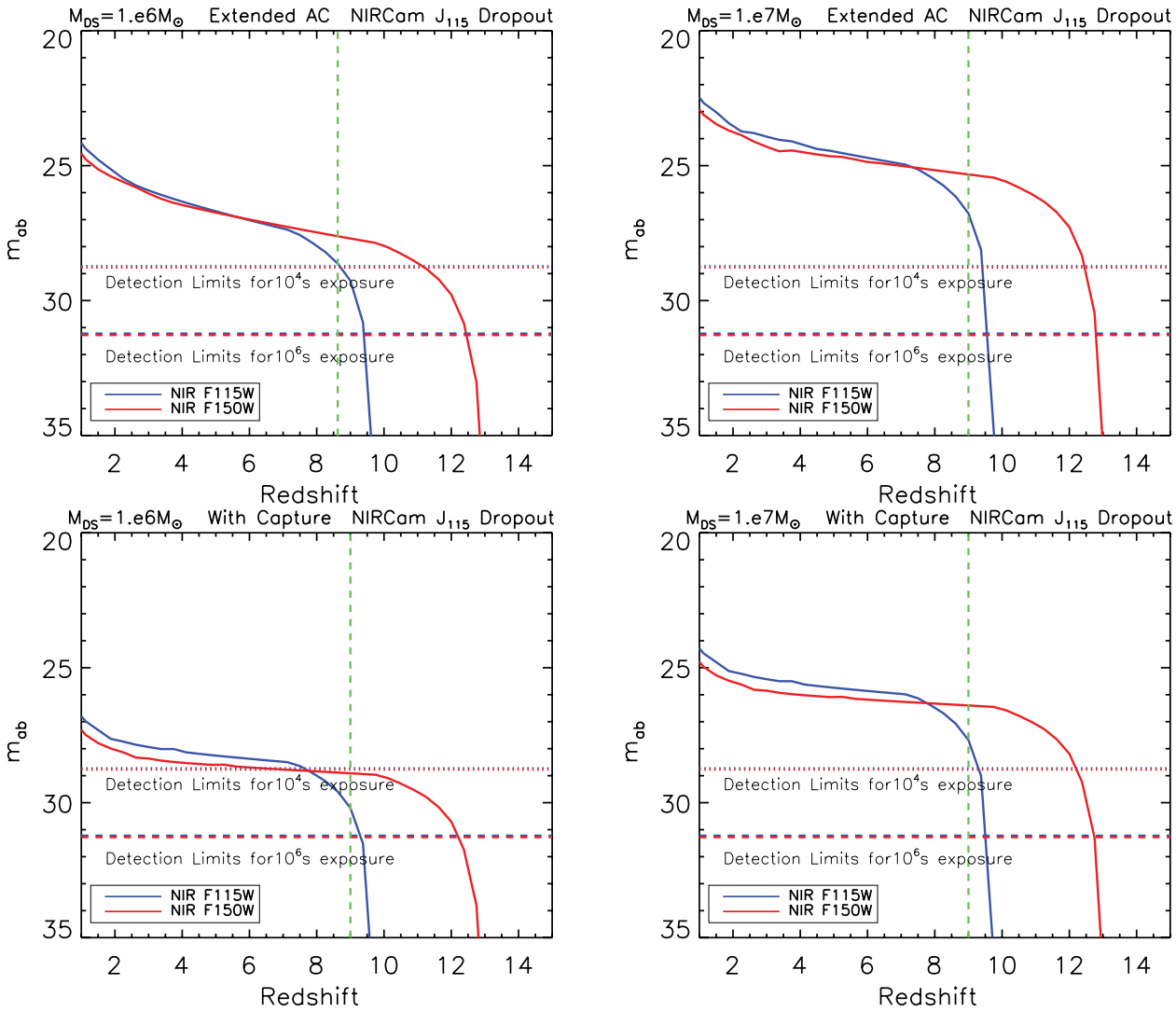

Figure 12. SMDS with *JWST* as J_{115}-band dropouts: apparent magnitudes for various SMDS through the $F115W$ and $F150W$ filters for NIRCam. Top panel: 10^6 and 10^7 $M_\odot$ DSs formed without DM capture. Lower panel: 10^6 and 10^7 $M_\odot$ DSs formed 'with capture'. The dotted horizontal lines are obtained from the 10σ required sensitivities for 10^4 s exposure data published at http://www.stsci.edu/jwst/instruments/nircam/; note that the detection limits for the J_{115} and the H_{150} filters differ by only $\sim$0.05 m_{AB} apparent magnitude and are thus essentially indistinguishable. The dashed horizontal lines are obtained assuming 10^6 s exposure time.

1.5×10^{-2} as our 'intermediate bounds' case. This case could imply that not all minihaloes host DS, or that not all DS survive throughout the $z \sim 10$ *HST* observability window. In this intermediate bounds case, hundreds or thousands of SMDSs are potentially observable.

For comparison, in the table we list as a third case the full number of DM haloes that could in principle host DS. If all of these contained DS, one would expect up to $\sim$450 000 DS with *JWST*. However, as discussed in Section 4.3, this would be extremely unreasonable as there would be no baryons outside of DS left for galaxy formation. Our results for the detectability of SMDS as H-band dropouts with *JWST* are summarized in Table 3.

5.3 Detection at $z \sim 15$ as a K_{200} dropout with *JWST*

DS at $z \gtrsim 14$ can be detected as K_{200}-band dropouts using the $F200$ and $F277$ NIRCam filters in *JWST*, as shown in Fig. 14 for 10^6 and 10^7 $M_\odot$ SMDS formed via extended AC (no capture) at $z_{form} = 20$. To qualify as a K_{200} dropout, the difference in magnitudes between the $F277W$ and $F200W$ filters must be greater than 1.2. As for the case of H-band dropouts above, we use *HST* data to bound the number of possible K-band dropouts, under three different assumptions: (i) maximal bounds, where every DS survives through the *HST* observability window at $z \sim 10$; (ii) intermediate bounds with $\sim 10^{-2}$ of the possible DS surviving that long and (iii) for comparison, simply counting every possible hosting halo. Our results for predicted numbers of SMDS observable as K-band dropouts with *JWST* are summarized in Table 4

The 10^6 $M_\odot$ DS could be observed in the redshift range $z \sim 15$–17 as a K_{200} dropout for 10^4 s exposure. For the case of maximal bounds from *HST*, we predict at most $N_{obs}^{multi} \sim 1$. For the intermediate bounds case, the possible number of detections is increased to roughly five for the case of a 9.68 arcmin^2 FOV or to 75 for the 150 arcmin^2 case. The (unreasonable) case where every possible halo hosts a DS shows the maximal number of 10^6 $M_\odot$ SMDS observable as K-band dropouts to be $\sim$70 000. In the case

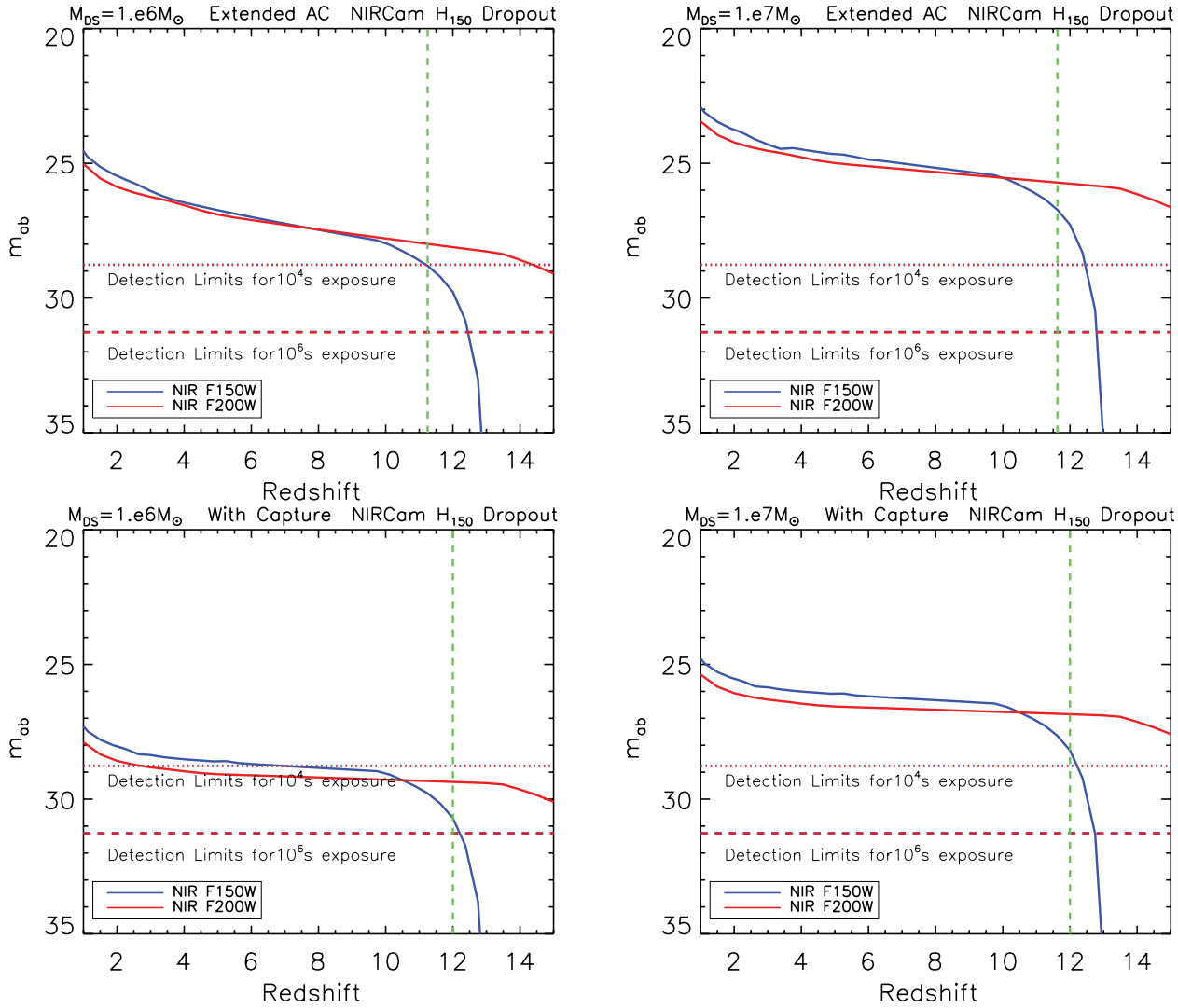

Figure 13. SMDS with *JWST* as H_{150}-band dropouts: apparent magnitudes for SMDS through the *F*150*W* and *F*200*W* NIRCam filters. Those could be used to establish dropout detection criteria in the 12–14 redshift range. Top panel: cases of interest (10^6 and 10^7 $M_\odot$) DSs formed without considering DM capture. Lower panel: 10^6 and 10^7 $M_\odot$ DSs formed including DM capture. The vertical green dashed line indicates the minimum redshift at which the DS will appear as a dropout.

of the 10^7 $M_\odot$ star, it would appear as a K_{200} dropout in the 16–20 redshift range. However, due to the sharp drop in the formation rate of DM haloes in the 1–2 $\times 10^8$ $M_\odot$ at such high redshift, the number of dropout events we predict in this case is at most $\sim$1 (other than for the unreasonable case where every single possible halo hosts an SMDS). The results for the detectability of SMDS as *K*-band dropouts with *JWST* are summarized in Table 4.

6 SMDS VERSUS POP III GALAXIES WITH *JWST*

A key question in the discovery of DSs with *JWST* will be the ability to differentiate these objects from other sources at high redshifts. Assuming that a population of potential $z > 10$ candidates is identified by the dropout techniques described in previous sections, the most significant contaminant population at these redshifts is likely to be galaxies dominated by Pop III stars. Indeed, Zackrisson et al. (2011a) and Pawlik, Milosavljevic & Bromm (2011) found that galaxies containing Pop III stars at high redshift are typically brighter in most *JWST* filters than later generations of stars; thus, galaxies with Pop III stars would be the most likely source of confusion in identifying DSs. In this section, we focus on ways to differentiate between SMDSs and galaxies containing Pop III stars.

Zackrisson et al. (2010a) showed that DSs in the mass range $<10^3$ $M_\odot$ could be easily distinguished from galaxies in the redshift range z = 0–15 (including galaxies containing Pop III stars), SNe, active galactic nuclei and Milky Way halo stars as well as Milky Way brown dwarfs by their extremely red colours in colour–colour plots. The DS considered there have all $T_{\rm eff} \lesssim$ 9000 K, which leads to a decrease of the ratio (*B*) of the fluxes to the left and right of the Balmer jump located at 0.365 μm with temperature (see section 8.3 of Rutten 2003). The significant Balmer jump in the case of DS with mass $\lesssim 10^3$ $M_\odot$ will lead to very red $m_{365} - m_{444}$ colours at $z = 10$, offering a distinct signature, as pointed out in Zackrisson et al. (2010a). Here we study instead the much heavier SMDSs with $M_{\rm DS} > 10^5$ $M_\odot$. These heavier stars are intrinsically much brighter and thus easier to find as dropouts.

Table 3. Upper limits on the number of SMDS detections as H_{150} dropouts with *JWST*. In the first three rows (labelled 'maximal bounds'), we assume that all the DSs live to below $z = 10$ where they would be observable by *HST*, and we apply the bounds on the numbers of DS $f_{\rm SMDS}$ from *HST* data in Section 4.2. The middle three rows (labelled 'intermediate') relax those bounds by assuming that only $\sim 10^{-2}$ of the possible DSs forming in $z = 12$ haloes make it through the *HST* observability window. For comparison, we also tabulate in the last three rows the total number of potential DM host haloes in each case. We also split the number of observations in two categories, $N_{\rm obs}^{\rm FOV}$ and $N_{\rm obs}^{\rm multi}$. The first assumes a sliver with the area equal to the FOV of the instrument (9.68 arcmin^2), whereas in the second we assume multiple field surveys with a total area of 150 arcmin^2. Note that for the case of the 10^7 M$_\odot$ SMDS the predictions are insensitive to the formation mechanism.

$M_{\rm DS}$ (M$_\odot$)	Formation scenario	Bounds from *HST*	$N_{\rm obs}^{\rm FOV}$	$N_{\rm obs}^{\rm multi}$
10^6	Extended AC	Maximal bounds	$\lesssim 1$	10
10^6	With capture	Maximal bounds	2	32
10^7	Any	Maximal bounds	$\lesssim 1$	~ 1
10^6	Extended AC	Intermediate	45	709
10^6	With capture	Intermediate	137	2128
10^7	Any	Intermediate	4	64
10^6	Extended AC	Number of DM haloes	28 700	444 750
10^6	With capture	Number of DM haloes	28 700	444 750
10^7	Any	Number of DM haloes	155	2400

Table 4. The number of SMDS detections as K_{200} dropouts with *JWST*. Cases are the same as above in Table 3.

$M_{\rm DS}$ (M$_\odot$)	Formation scenario	Bounds from *HST*	$N_{\rm obs}^{\rm FOV}$	$N_{\rm obs}^{\rm multi}$
10^6	Extended AC	Maximal bounds	$\lesssim 1$	~ 1
10^7	Any	Maximal bounds	$\ll 1$	$\ll 1$
10^6	Extended AC	Intermediate	5	75
10^7	Any	Intermediate	$\ll 1$	$\lesssim 1$
10^6	Extended AC	Number of DM haloes	4511	69 900
10^7	Any	Number of DM haloes	8	116

However, they are also hotter than 10 000 K, leading to values of the ratio B to increase with temperature, as explained in section 8.3 of Rutten (2003). For the SMDS, we consider here the Balmer jump is insignificant, therefore it is much more difficult distinguishing them from potential interlopers based on the technique proposed in Zackrisson et al. (2010a) for the smaller $\sim 10^3$ M$_\odot$ DS. In this section, we begin a discussion of this issue, restricting our studies to what can be learned from *JWST* directly. Future studies will be required, in which we investigate also the possible role of spectroscopy with TMT and GMT, and other upcoming observatories in differentiating Pop III galaxies from DSs.

The earliest Pop III stars (in the absence of DM heating) are expected to have masses in the range 10–100 M$_\odot$ – too faint to be seen as individual objects with *JWST* (Oh 1999; Oh, Haiman & Rees 2001; Gardner et al. 2006; Rydberg, Zackrisson & Scott 2010). However, a galaxy containing 10^5–10^7 M$_\odot$ of Pop III stars might indeed be detectable. Zackrisson et al. (2011a) presented a comprehensive study of the integrated spectra signatures of Pop III stars in the wide filters of *JWST*. Their main findings are that Pop III galaxies could be detectable to redshifts as high as 20 if the stellar population mass is $\sim 10^7$ M$_\odot$ (or in the case of 10^5 M$_\odot$ stellar population mass up to redshifts of 10). A similar study by Pawlik et al. (2011), who examined nebular emission lines from early galaxies, came to the same conclusion: thousands of these may be found with *JWST*. Moreover, Inoue et al. (2011) and Zackrisson et al. (2011a) have proposed selection criteria using two of the filters of *JWST*: Inoue et al. (2011) argued for using two NIRCam filters and Zackrisson et al. (2011a) argued for adding imaging in two MIRI filters to more cleanly differentiate between Pop III galaxies and Pop II or Pop I galaxies at $z \sim 7$–8. As mentioned above, these authors found that galaxies containing Pop III stars at high redshift are typically brighter in most *JWST* filters than galaxies containing Pop I or Pop II stars; thus, galaxies with Pop III stars would be the most likely source of confusion in identifying DSs.

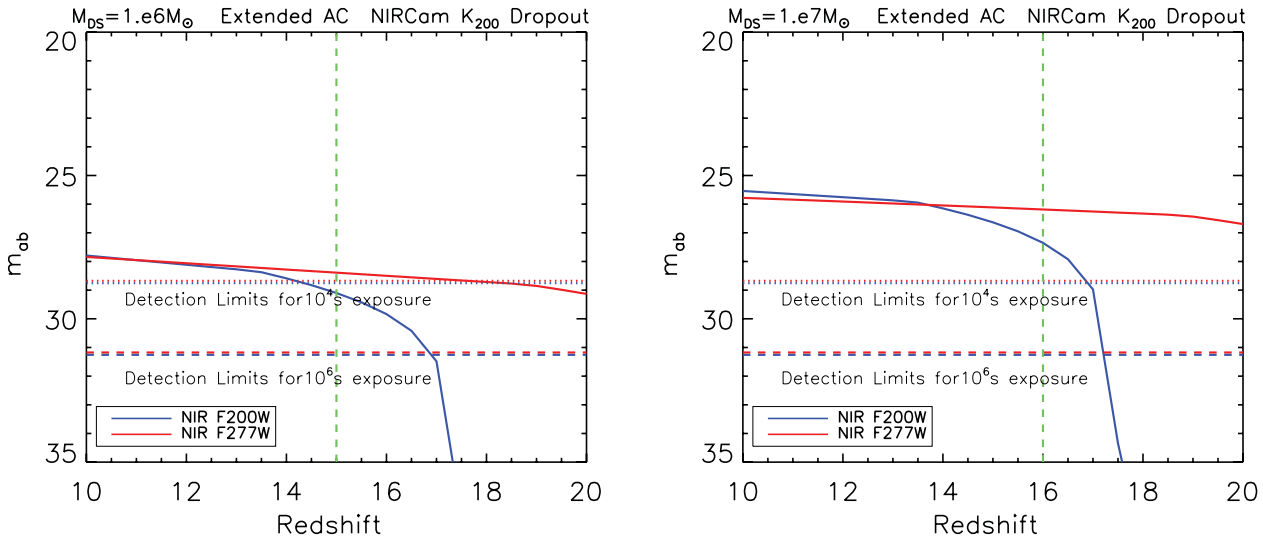

Figure 14. SMDS with *JWST* as K_{200}-band dropouts: apparent magnitudes for SMDS formed without DM capture through the *F*200*W* and *F*277*W* NIRCam filters. Left-hand panel: for the 10^6 M$_\odot$ DS. Right-hand panel: for the 10^7 M$_\odot$ DS. The vertical green dashed line indicates the minimum redshift at which the DS will appear as a dropout.

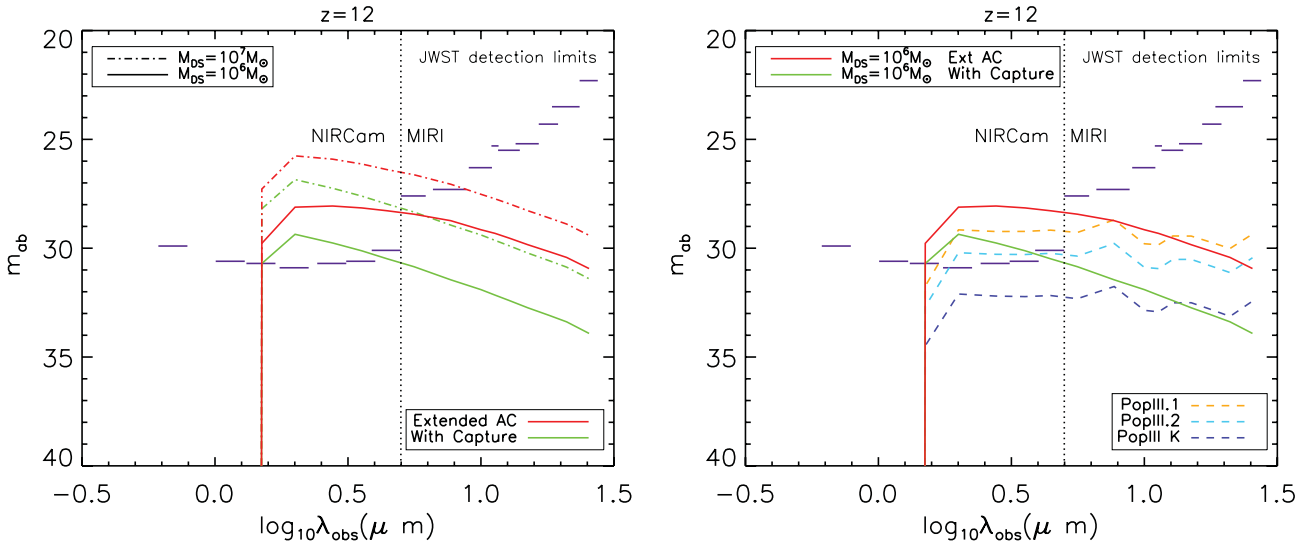

Figure 15. *JWST* detection limits and apparent magnitudes of SMDS and Pop III galaxies. Each filter's sensitivity limit for *JWST* NIRCam and MIRI wide filters for 100 h of exposure time is plotted as a segment at the corresponding wavelength. Left-hand panel: apparent magnitudes for SMDS in the 10^6 $M_\odot$ (solid lines) to 10^7 $M_\odot$ (dot–dashed lines) mass range for both extended AC (red lines) and capture (green lines) formation mechanisms. Right-hand panel: apparent magnitudes of SMDS of 10^6 $M_\odot$ (solid lines) and Pop III instantaneous burst galaxies of 1 Myr age (dashed lines) with the same stellar population mass as the SMDS.

Using the YGGDRASIL[4] model grids (Zackrisson et al. 2011a, see http://ttt.astro.su.se/~ez/), we compare signatures in the NIRCam passbands of Pop III galaxies at $z \sim 10$–15 with those of SMDS. All the nomenclature used here for Pop III galaxies follows Zackrisson et al. (2011a): we consider the following three different IMFs for Pop III galaxies.

(i) *Pop III.1*. A zero-metallicity population with an extremely top-heavy IMF and a single stellar population (SSP) from Schaerer (2002) with a power-law IMF ($dN/dM \propto M^{-\alpha}$). The population has stellar masses in the range 50–500 $M_\odot$ and a Salpeter slope $\alpha = 2.35$ for the entire mass range.

(ii) *Pop III.2*. A zero-metallicity population with a moderately top-heavy IMF. An SSP from Raiter, Schaerer & Fosbury (2010) is used. This model has a lognormal IMF with characteristic mass $M_c = 10\,M_\odot$ and dispersion $\sigma = 1\,M_\odot$. The wings of the mass function extend from 1 to 500 $M_\odot$.

(iii) *Pop III, Kroupa IMF*. In view of recent simulations (e.g. Greif et al. 2010), the mass of Pop III stars might be lower than previously predicted. Therefore, in this case a normal Kroupa (2001) IMF, usually describing Pop II/I galaxies, is used. The stellar masses range from 0.1 to 100 $M_\odot$ and the SSP is a rescaled version of the one used in Schaerer (2002).

Following Zackrisson et al. (2011a), we further subdivide the models into two types, based on the amount of nebular emission. The first galaxies are expected to have significant ionized gas surrounding them. Depending on how compact the H II region is, the escape fraction for ionizing radiation from the galaxy into the IGM can vary anywhere from 0 to 1. Hence, we consider the following two extreme possibilities.

(i) *Type A galaxies*. If the gas covering fraction $f_{cov} = 1$, then there is maximal nebular contribution to the SED and no escape of Lyman continuum photons.

(ii) *Type C galaxies*. If $f_{cov} = 0$, there is no nebular contribution to the SEDs and instead stellar light dominates the SED. We will not consider here the intermediate case of Type B galaxies.

Zackrisson et al. (2011a) argue that the nebular emission typically dominates the spectrum of young Pop III galaxies at $z \sim 10$–15; e.g. at $z = 10$, nebular emission dominates for galaxies younger than 10 Myr (see also Zackrisson, Bergvall & Leitet 2008). All young or star-forming galaxies are expected to have significant contribution to the SEDs from nebular emission, and this effect is increased with lower metallicity or a more pronounced top-heavy IMF. Hence, we will predominantly focus on case A of maximal nebular emission from the early galaxies.

In another paper, Zackrisson (2011) investigates the possibility of nebular emission from the hottest DSs, those with $T_{eff} > 30\,000$ K, which have the possibility of photoionizing the gas in their host haloes, thereby producing bright H II regions which could substantially boost the observed fluxes of these stars. Indeed, Zackrisson (2011) shows that nebular emission from SMDS may boost the *H*-band fluxes of these stars by up to roughly 1 mag at $z \sim 10$ and roughly 2 mag at lower redshifts. Such nebular emission would clearly modify the SMDS spectra as well. However, as noted in that same paper, there is not likely to be much gas left in the halo to form an ionization bounded nebula; the SMDSs have already accreted most of the baryons within the virial radius of the halo, leaving a very low-density nebula. In addition, any remaining gas may eventually be ejected from the halo (Alvarez et al. 2006) to form a huge, low surface brightness nebula in the IGM, with little effect on observations of SMDSs. Thus, in this paper, we ignore the possibility of nebular emission from SMDSs.

In Fig. 15, we plot the SEDs (in apparent magnitudes) of SMDS and Pop III galaxies at $z = 12$ as a function wavelength. Our interest is in their detectability with the NIRCam and MIRI cameras on *JWST*. The vertical dotted line demarcates the wavelength ranges covered by the two instruments, and the dark blue horizontal segments represent band widths and the sensitivity limits of individual

[4] We highly recommend watching the movie Thor to understand this name.

filters assuming a 100 h exposure.[5] In the left-hand panel, we plot the apparent magnitudes for 10^6 and 10^7 $M_\odot$ DS formed via both extended AC and capture mechanisms. We have previously discussed (see Figs 10 and 11) that both 10^6 and 10^7 $M_\odot$ DS are bright enough to be observed by the NIRCam filters. On the other hand, in the less sensitive MIRI filters, 10^7 $M_\odot$ DS can be seen in the lowest two wavelength filters (*F*560*W* and *F*770*W*) but 10^6 $M_\odot$ DS are too faint to be observed.

In the right-hand panel, we compare the observed SEDs of 10^6 $M_\odot$ SMDS (solid curves) with Pop III galaxies (dashed curves). For the galaxies, we assumed an instantaneous starburst (at $t = 0$) and used the results from the YGGDRASIL code at 1 Myr after the burst. The light from the galaxies is assumed to be dominated by nebular emission (type A; Zackrisson et al. 2011a) for galaxies younger than 10 Myr. We have taken the stellar mass of the galaxy to be the same value 10^6 $M_\odot$ as the DS mass. SMDS are brighter than the galaxies in all filters in which the objects are potentially visible. The sharp cut-off in flux at $\log_{10}\lambda_{\rm obs} \sim 0.02$ is due to Lyα absorption. For a stellar population mass of 10^6 $M_\odot$, Pop III.1 galaxies are detectable as a H_{150} dropouts in a deep field survey with an exposure of 100 h; Pop III.2 are still just above the sensitivity limits; but Pop III galaxies with a Kroupa IMF are not detectable as H_{150} dropouts.

Let us imagine that an object has been detected as a photometric dropout at some redshift, say an *H*-band dropout at $z = 12$. Our goal is to determine the nature of this object, i.e. to differentiate SMDS from first galaxies with *JWST*. One approach would be to exploit the emission lines in galaxies that are not shared by the DS. Pawlik et al. (2011) have shown that there would be several major signatures in the spectra for Pop III galaxies with significant nebular emission (our case A), including the He II line at 0.1640 μm and Hα emission. They found that *JWST* spectrometers (NIRSpec and MIRI) are indeed sensitive enough to detect these emission lines, thereby potentially finding up to tens of thousands of starbursting galaxies with redshifts $z \geq 10$ in its FOV of $\sim$10 arcmin^2. They also found that the He 1640 recombination line is only detectable in significant numbers for the case of zero-metallicity starbursts with top-heavy IMF. They noted that their estimates are consistent with previous estimates of *JWST* starburst counts (e.g. Haiman & Loeb 1998; Oh 1999). A third possibility would be to detect the continuum limit of the Balmer series at 0.3646 μm in the rest frame.

In short, if follow-up spectroscopy is done on an object found as dropout with *JWST*, the detection of an He II 1640 emission line or an Hα emission line would most likely indicate that the object is a Pop III galaxy with nebular emission rather than an SMDS (later stellar populations e.g. Pop II would also be missing these emission lines, but would not be as bright as either Pop III galaxies or SMDSs). We do, however, note one caveat: if there is any SN explosion that can result from the end of SMDS evolution, there might be another way to make He II 1640 radiation. When the SN remnant shock reaches the radiatively cooling stage of its evolution (i.e. when post-shock gas cools radiatively faster than it does by adiabatic expansion), the shock becomes a 'radiative shock', and that usually means that gas cools from a post-shock temperature above a million degrees, down to 10^4 K or below, and He II line emission will also occur. The shocks that do this need not only be SN explosion shocks, but could also be halo virialization shocks, for haloes large enough to have virial *T* high enough to ionize He II to He III. On the other hand, as discussed above, Heger (personal communication) finds that (in the absence of rotation) fusion-powered stars more massive than 153 000 $M_\odot$ collapse directly to supermassive BH seeds rather than blowing up as SN.

While the detection of emission lines most likely indicates that the object is a Pop III galaxy rather than an SMDS, the lack of emission lines leaves both possibilities still open. One might therefore ask how well the underlying continuum spectrum can be determined with *JWST*. The UV continuum slopes for galaxies in the redshift range 2–8 have been analysed using *HST* data in the literature (e.g. Bouwens et al. 2009, 2010; Dunlop et al. 2011; Finkelstein et al. 2011; McLure et al. 2011). The value of β can be determined by converting photometric colours in relevant filters [as in Bouwens et al. (2010) or Dunlop et al. (2011) for *HST*], but as noted in McLure et al. (2011) the photometric errors can be quite large. A detailed study of how well this separation can be done based on UV spectra is the subject of future work.

The He II line in Pop III type A galaxies due to nebular emission at 0.1640 μm would fall within the *F*200*W* filter of *JWST* for sources at redshifts $9.7 < z < 12.7$. The strength of the line is modelled in the YGGDRASIL code for all Pop III galaxies we have considered. Since this line is pronounced in Pop III galaxies but not in DS, one could examine the difference in the two magnitudes $m_{150} - m_{200}$, which would be significantly more negative (i.e. bluer $m_{150} - m_{200}$ colours) for DS than for the galaxies. One should be able to see this effect for objects at $z < 12$. At higher redshifts, however, the Gunn–Peterson cuts off significantly the fluxes in the *F*150*W* filter, so that it would be impossible to distinguish an increase of *F*200*W* flux (due to He II in Pop III galaxies) from a decrease of *F*150*W* flux (due to Lyα absorption).

Another approach to distinguish between different types of objects is their location in colour/colour plots. Previously, Inoue et al. (2011) and Zackrisson et al. (2011a) used colour/colour plots to distinguish between different types of galaxies: those with Pop III.1 stars versus those containing a later population of stars. In Fig. 16, we try out the possibility of differentiating DS versus galaxies, based on their locations in colour/colour plots. In the left- and right-hand panels, we study Pop III instantaneous burst galaxies of type A (maximal nebular emission) and type C (no nebular emission), respectively. We focus here on objects at $z = 12$ as this is the most favourable redshift to look for SMDSs. The empty circle (cross) symbols correspond to magnitudes for SMDS of 10^6 $M_\odot$ (10^7 $M_\odot$). The solid lines represent the evolutionary tracks of Pop III galaxies obtained using the YGGDRASIL model grids, with points marking three different ages (diamonds for 1Myr, triangles for 3 Myr, and squares for 10 Myr). We note that, due to the similar temperatures, SMDS formed 'with capture' of either 10^6 or 10^7 $M_\odot$ occupy the same spot on the diagrams.

Pop IIIA galaxies with lifetimes less than 10 Myr will exhibit redder colours than SMDS in the $m_{356} - m_{444}$ (see lower left-hand panel) due to the increased fluxes in the *F*444*W* filter due to the Balmer emission lines from the galaxies. One might therefore hope that to distinguish between SMDS and Pop III type A galaxies at $z \sim 12$ would be to look for red colours in $m_{356} - m_{444}$. Indeed, for the case in Fig. 16, this technique would work: only the Pop III.1 galaxies are bright enough to compete with SMDS (see Fig. 15), yet these are in a distinctly different location on the colour/colour plot from the SMDS. However, in the figure we have taken the stellar mass of the galaxies to be 10^6 $M_\odot$, while this number could be an order of magnitude higher, which would drive the Pop III lines in the figure closer to the SMDSs. In future work, we plan to investigate how well this differentiation can be done in various instruments.

[5] For NIRCam, we did not plot the *F*090*W* filter, since the throughput profile is not yet available.

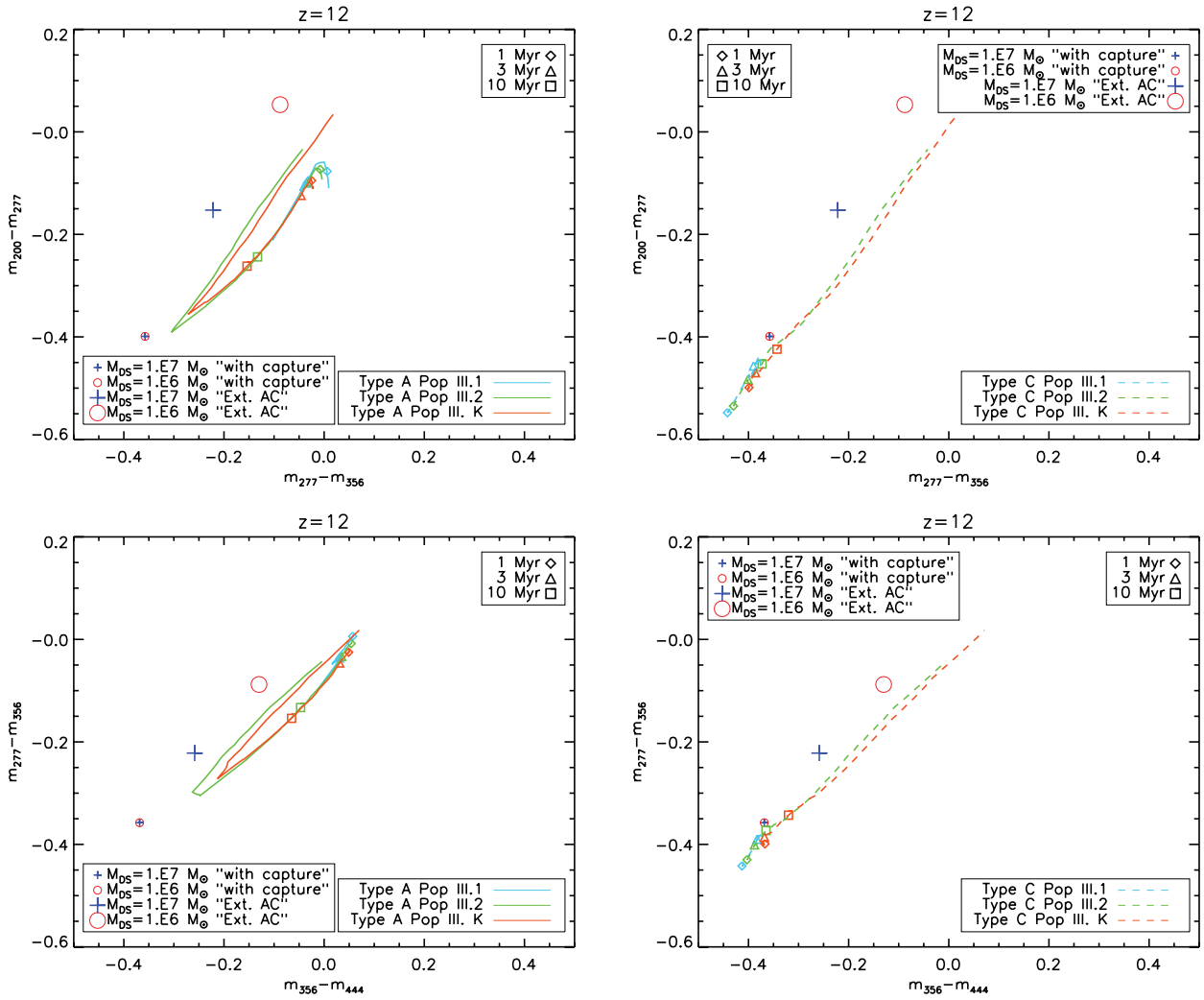

Figure 16. Signatures of SMDS and instantaneous burst Pop III galaxies in $m_{277} - m_{356}$ versus $m_{200} - m_{277}$ (top row) and $m_{356} - m_{444}$ versus $m_{277} - m_{356}$ (bottom row) colour diagrams. The left-hand column corresponds to type A Pop III galaxies (maximal nebular emission) and the right-hand column to type C Pop III galaxies (no nebular emission). The solid lines are evolutionary tracks for Pop III galaxies obtained using the YGGDRASIL model grids introduced in Zackrisson et al. (2011a). The points along the evolutionary tracks single out the evolution at three different ages of the galaxies. 10^6 M$_\odot$ (10^7 M$_\odot$) SMDS are represented by circle (cross) symbols in the diagrams. For the extended AC case, we chose a larger size symbol compared to the SMDS formed 'with capture'.

Differentiating between SMDS and galaxies containing Pop III galaxies is an important issue. Using *JWST*, the best bet is to look for emission lines of He 1640 or Hα. If these are found, the object is not likely to be an SMDS. On the other hand, if these are not found, then differentiation via the continuum slope or colour/colour plots may be feasible and is the study of future research. Studies with other instruments, specifically ground-based spectrometers, may prove to be helpful.

7 SUMMARY AND CONCLUSIONS

The first phase of stellar evolution may have been DSs, powered by DM annihilation. These form inside early 10^6–10^8 M$_\odot$ haloes at $z = 10$–50. Initially, DS are puffy objects with masses of 1–10 M$_\odot$ and radii $\sim$10 au. As long as they are DM powered, their surface temperatures ($\sim 10^4$ K) remain cool enough to allow continued growth via accretion of baryons until they become supermassive $M_{\rm SMDS} \sim 10^6$ or 10^7 M$_\odot$. The requisite DM fuel can be acquired in two ways: (i) extended AC due to DM particles on chaotic or box orbits in triaxial haloes and (ii) capture of DM particles via elastic scattering off nuclei in the star. In this paper, we have studied the detectability of SMDS formed via both mechanisms with upcoming *JWST* observations.

In order to determine their observational characteristics, we obtained the spectra of SMDSs with the TLUSTY stellar atmospheres code (Fig. 1). We used *N*-body simulations for structure formation at high redshifts (Iliev et al. 2010) to obtain estimates for the numbers of DM haloes capable of hosting SMDS (Fig. 2 and Table 1). Then we used *HST* observations to set limits on their detectability.

Both 10^6 and 10^7 M$_\odot$ SMDS could be seen in *HST* data and would be detected as *J*-band dropouts. Since Bouwens et al. (2011) report only one plausible $z \sim 10$ object in the data, we used the fact that at most one observable DS at this redshift can exist to obtain bounds on the possible numbers of DS in equations (11) and (12).

SMDSs are bright enough to be seen in all the wavelength bands of the NIRCam on *JWST*, while detection is more difficult in the less sensitive higher wavelength MIRI camera. We showed that SMDSs could be seen as *J*-, *H*- or *K*-band dropouts, which would identify them as $z \sim 10$, 12 and 14 objects, respectively.

The strong point of *JWST* will be its sensitivity to longer wavelengths than *HST*, corresponding to light from higher redshifts where SMDSs may be found. While *JWST* is not particularly better than *HST* at finding *J*-band dropouts, it will be significantly better at finding SMDS as *H*- and *K*-band dropouts.

We can summarize our predictions for the numbers of SMDS seen as *H*-band dropouts with *JWST* as

$$N_{\rm obs} = 4.4 \times 10^5 f_{\rm smds} f_{\Delta t} (\theta/150\,{\rm arcmin})^2 \qquad (M_{\rm DS} = 10^6\,{\rm M}_\odot), \tag{13}$$

$$N_{\rm obs} = 2.4 \times 10^3 f_{\rm smds} f_{\Delta t} (\theta/150\,{\rm arcmin})^2 \qquad (M_{\rm DS} = 10^7\,{\rm M}_\odot), \tag{14}$$

where we have scaled the results to 150 arcmin^2 survey area, which would require multiple surveys by *JWST*.

Similarly, our predictions for the numbers of SMDS seen as *K*-band dropouts are

$$N_{\rm obs} = 7 \times 10^4 f_{\rm smds} f_{\Delta t} (\theta/150\,{\rm arcmin})^2 \quad (M_{\rm DS} = 10^6\,{\rm M}_\odot, {\rm AC}), \tag{15}$$

$$N_{\rm obs} = 120 f_{\rm smds} f_{\Delta t} (\theta/150\,{\rm arcmin})^2 \quad (M_{\rm DS} = 10^7\,{\rm M}_\odot). \tag{16}$$

$10^6\,{\rm M}_\odot$ SMDS formed via capture are not detectable.

Although these numbers are quite large, as we have emphasized throughout, it is quite likely that $f_{\rm SMDS} f_{\Delta t} \ll 1$. If the DS survives to $z \sim 10$, *HST* observations bound this product. Our final predictions for numbers of SMDS that could be detected by *JWST* are found in Tables 3 and 4.

Differentiating between SMDS and galaxies containing metal-free Pop III stars is an important issue, and we have begun an investigation of this question here. Galaxies containing later generations of stars are not as bright and not a source of confusion. Using *JWST*, the best bet to differentiate SMDS from Pop III galaxies is to look for emission lines of He 1640 or Hα. If these are found, the object is not likely to be an SMDS. On the other hand, if these are not found, then differentiation via the continuum slope or colour/colour plots may be feasible and is the study of future research. Further estimates should also be done using instruments such as GMT, TMT, LSST and others.

SMDS can play an important role in the formation of supermassive BHs in the Universe. As argued by Heger (private communication), in the absence of a DS phase, the characteristic mass for big BHs at birth is 153 000 $\rm M_\odot$ (i.e. once a fusion-powered star accretes this much mass, it can no longer sustain hydrostatic equilibrium and collapses directly to a BH). With a DS phase, the DS could instead grow to a larger mass while DM powered, and then collapse directly to a BH; thus, in this case the BH could be born with larger masses. Future observations of large BHs might thus be able to differentiate someday between formation mechanisms via DSs or fusion-powered stars.

In an interesting recent paper, Maurer et al. (2012) discussed the contribution of DS light to the IR background and compared with a number of observations. They studied only DS with masses less than $1000\,{\rm M}_\odot$ and found bounds that are not very strong unless these objects live for a billion years (not very likely for these objects). In the future, it will be interesting to examine the same effect for the heavier SMDS.

SMDS mass as a function of halo mass. Although we have assumed in this paper that DS grow to the point where they consume most of the baryons in the haloes that host them, one can examine how the results would change if we were to stop the growth at a smaller fraction of the total baryonic content. For the case of 'maximal bounds', we can show that the resulting predictions for *JWST* remain identical. For example, the case we considered in the paper of $10^6\,{\rm M}_\odot$ SMDS that grew inside $\sim 10^7\,{\rm M}_\odot$ haloes can be compared instead to the case of $10^6\,{\rm M}_\odot$ SMDS that grew inside $\sim 10^8\,{\rm M}_\odot$ haloes. For the case of 'maximal bounds', which assumes that *HST* bounds at $z = 10$ apply directly to SMDS at $z = 12$ (i.e. that the SMDS at $z = 12$ survive all the way to $z = 10$), we find that our results are completely unchanged. The number of $10^8\,{\rm M}_\odot$ haloes is smaller than the number of $10^7\,{\rm M}_\odot$ haloes both at redshifts $z = 10$ (so the *HST* bounds are weaker) and at $z = 12$ (where the *JWST* observations are made). Thus, the two effects cancel exactly. One can see this cancellation in the following way. The numbers of SMDS observable in either *HST* or *JWST* are given by the same equation, equation (9). The two factors ${\rm d}N/{\rm d}z{\rm d}\theta^2$ and $f_{\rm SMDS}(z = z_{\rm start})$ change depending on the hosting halo mass, but their product remains the same since it is set by *HST* bounds in equation (10). Thus, the numbers with *JWST* are unchanged regardless of halo size.

The current decade is a time of great excitement in the physics community regarding the possibility of detection of the DM particle. Three approaches are being pursued in the hunt for WIMPs: direct detection (including DAMA, CDMS, XENON, COGENT, CRESST, ZEPLIN, TEXONO, COUPP and many others worldwide), indirect detection (including *PAMELA*, *Fermi*, IceCube) and colliders (LHC). Many of these experiments have indeed found hints of a signal, though confirmation in more than one type of detector of the same particle remains a goal. DSs offer a fourth possibility for the discovery of WIMPs, or of learning about their properties. If WIMPs are indeed discovered, then it is very reasonable to expect to find DSs in the sky that are WIMP powered. It is even possible that the WIMPs have the property that they will be seen first by *JWST* before any other experiment. In either case, the prospect of finding a new type of star in the next premier NASA mission is greatly exciting.

ACKNOWLEDGMENTS

We are extremely grateful to Pat Scott for providing spectra for DSs with the TLUSTY code and to E. Zackrisson for making the YGGDRASIL model grids publicly available. This research is supported in part by Department of Energy (DOE) grant number DE-FG02-95ER40899 and by the Michigan Center for Theoretical Physics. KF thanks the Texas Cosmology Center (TCC) where she was a Distinguished Visiting Professor. TCC is supported by the College of Natural Sciences and the Department of Astronomy at the University of Texas at Austin and the McDonald Observatory. KF also thanks the Aspen Center for Physics for hospitality during her visit. MV acknowledges support from NSF grant number AST-0908346. ITI acknowledges support from the Southeast Physics Network (SEPNet) and the Science and Technology Facilities Council grant number ST/I000976/1. PRS acknowledges support from NSF grant AST-1009799 and NASA grant NNX11AE09G. The authors acknowledge the Texas Advanced Computing Center (TACC) at The University of Texas at Austin for providing HPC resources that have contributed to the research results reported within this paper (http://www.tacc.utexas.edu).

REFERENCES

Aalseth C. E. et al., 2011, Phys. Rev. Lett., 107, 141301
Abdo A. A. et al., 2009a, Phys. Rev. Lett., 103, 251101

Abdo A. A. et al., 2009b, Phys. Rev. Lett., 102, 181101
Abdo A. A. et al., 2010, J. Cosmol. Astropart. Phys., 1004, 014
Adriani O. et al., 2009, Phys. Rev. Lett., 102, 051101
Adriani O. et al., 2010, Astropart. Phys., 34, 1
Alvarez M. A., Bromm V., Shapiro P. R., 2006, ApJ, 639, 621
Angloher G. et al., 2011, preprint (arXiv:1109.0702)
Barkana R., Loeb A., 2001, Phys. Rep., 349, 125
Begelman M. C., Volonteri M., Rees M. J., 2006, MNRAS, 370, 289
Bernabei R. et al., 2010, in Cecchi C., Ciprini S., Lubrano P., Tosti G., eds, AIP Conf. Ser. Vol. 1223. Am. Inst. Phys., New York, p. 50
Bertone G., Fairbairn M., 2008, Phys. Rev. D, 77, 043515
Bouquet A., Salati P., 1989, ApJ, 346, 284
Bouwens R. J., Illingworth G. D., Blakeslee J. P., Franx M., 2006, ApJ, 653, 53
Bouwens R. J. et al., 2009, ApJ, 705, 936
Bouwens R. J. et al., 2010, ApJ, 708, L69
Bouwens R. J. et al., 2011, Nat, 469, 504
Bromm V., Larson R. B., 2004, ARA&A, 42, 79
Bromm V., Yoshida N., Hernquist L., McKee C. F., 2009, Nat, 459, 49
Casanellas J., Lopes I., 2009, ApJ, 705, 135
Casanellas J., Lopes I., 2011, ApJ, 733, L51
Clark P. C., Glover S. C. O., Klessen R. S., Bromm V., 2011, ApJ, 727, 110
Dobler G., Finkbeiner D. P., Cholis I., Slatyer T., Weiner N., 2010, ApJ, 717, 825
Drukier A. K., Freese K., Spergel D. N., 1986, Phys. Rev. D, 33, 3495
Dunlop J. S., McLure R. J., Robertson B. E., Ellis R. S., Stark D. P., Cirasuolo M., de Ravel L., 2011, MNRAS, 420, 901
Fan X. et al., 2001, AJ, 121, 31
Fan X. et al., 2004, AJ, 128, 515
Fan X. et al., 2006, AJ, 131, 1203
Finkelstein S. L. et al., 2011, preprint (arXiv:1110.3785)
Freese K., Frieman J. A., Gould A., 1988, Phys. Rev. D, 37, 3388
Freese K., Bodenheimer P., Spolyar D., Gondolo P., 2008a, ApJ, 685, L101
Freese K., Spolyar D., Aguirre A., 2008b, J. Cosmol. Astropart. Phys., 0811, 014
Freese K., Gondolo P., Sellwood J. A., Spolyar D., 2009, ApJ, 693, 1563
Freese K., Ilie C., Spolyar D., Valluri M., Bodenheimer P., 2010a, ApJ, 716, 1397
Freese K. et al., 2010b, AIP Conf. Proc. Vol. 1294, First Stars and Galaxies Conference, Austin, TX. Am. Inst. Phys., New York, p. 45
Gardner J. P. et al., 2006, Space Sci. Rev., 123, 485
Gondolo P., Huh J.-H., Kim H. D., Scopel S., 2010, preprint (arXiv:1004.1258)
Greif T. H., Glover S. C. O., Bromm V., Klessen R. S., 2010, ApJ, 716, 510
Greif T. H., Springel V., White S. D. M., Glover S. C. O., Clark P. C., Smith R. J., Klessen R. S., Bromm V., 2011a, ApJ, 737, 75
Greif T. H., White S. D. M., Klessen R. S., Springel V., 2011b, ApJ, 736, 147
Grogin N. A. et al., 2011, ApJS, 197, 35
Haiman Z., Loeb A., 1998, ApJ, 503, 505
Haiman Z., Loeb A., 2001, ApJ, 552, 459
Heger A., Woosley S. E., 2002, ApJ, 567, 532
Hirano S., Umeda H., Yoshida N., 2011, ApJ, 736, 58
Hooper D., Spolyar D., Vallinotto A., Gnedin N. Y., 2010, Phys. Rev. D, 81, 103531
Hubeny I., 1988, Comput. Phys. Communications, 52, 103
Ilie C., Freese K., Spolyar D., 2011, New J. Phys., 13, 053050
Iliev I. T., Mellema G., Shapiro P. R., Pen U.-L., 2007, MNRAS, 376, 534
Iliev I. T., Ahn K., Koda J., Shapiro P. R., Pen U., 2010, preprint (arXiv:1005.2502)
Inoue A. K. et al., 2011, MNRAS, 411, 2336
Iocco F., 2008, ApJ, 677, L1
Iocco F., 2010, in Proc. Sci., CRF2010, 018
Iocco F. et al., 2008, MNRAS, 390, 1655
Koekemoer A. M. et al., 2011, ApJS, 197, 36
Komatsu E. et al., 2009, ApJS, 180, 330
Komatsu E. et al., 2011, ApJS, 192, 18
Krauss L. M., Freese K., Press W., Spergel D., 1985, ApJ, 299, 1001
Kroupa P., 2001, MNRAS, 322, 231
Lodato G., Natarajan P., 2006, MNRAS, 371, 1813
Loeb A., Rasio F. A., 1994, ApJ, 432, 52
McKee C. F., Tan J. C., 2008, ApJ, 681, 771
McLure R. J. et al., 2011, preprint (arXiv:1102.4881)
Maurer A., Raue M., Kneiske T., Horns D., Elsässer D., Hauschildt P. H., 2012, ApJ, 745, 166
Merz H., Pen U.-L., Trac H., 2005, New Astron., 10, 393
Moskalenko I. V., Wai L. L., 2007, ApJ, 659, L29
Narayan R., Piran T., Kumar P., 2001, ApJ, 557, 949
Natarajan A., Tan J. C., O'Shea B. W., 2009, ApJ, 692, 574
Oesch P. A. et al., 2012, ApJ, 745, 110
Oh S. P., 1999, ApJ, 527, 16
Oh S. P., Haiman Z., Rees M. J., 2001, ApJ, 553, 73
Pawlik A. H., Milosavljevic M., Bromm V., 2011, ApJ, 731, 54
Press W. H., Spergel D. N., 1985, ApJ, 296, 679
Raiter A., Schaerer D., Fosbury R. A. E., 2010, A&A, 523, A64
Ripamonti E., Abel T., 2005, preprint (astro-ph/0507130)
Ripamonti E. et al., 2009, PoS, IDM2008, 075, SISSA, Trieste
Ripamonti E., Iocco F., Ferrara A., Schneider R., Bressan A., Margio P., 2010, MNRAS, 406, 2605
Rutten R. J., 2003, Radiative Transfer in Stellar Atmospheres. Ulrecht University Lecture Notes, Ulrecht
Rydberg C. E., Zackrisson E., Scott P., 2010, in Raue M., Kneiske T., Horns D., Elsaesser D., Hauschildt P., eds, Cosmic Radiation Fields 2010, Sources in the Early Universe. PoS CRF2010, 026, SISSA, Trieste
Salati P., Silk J., 1989, ApJ, 338, 24
Sandick P., Diemand J., Freese K., Spolyar D., 2011, J. Cosmol. Astropart. Phys., 1, 18
Schaerer D., 2002, A&A, 382, 28
Schleicher D. R. G., Banerjee R., Klessen R. S., 2008, Phys. Rev. D, 78, 083005
Schleicher D. R. G., Banerjee R., Klessen R. S., 2009, Phys. Rev. D, 79, 043510
Scott P., 2010, in Raue M., Kneiske T., Horns D., Elsaesser D., Hauschildt P., eds, Cosmic Radiation Fields 2010, Sources in the Early Universe. PoS, CRF2010, 021, SISSA, Trieste
Scott P., Edsjö J., Fairbairn M., 2007, preprint (arXiv:0711.0991)
Scott P., Fairbairn M., Edsjo J., 2008, MNRAS, 394, 82
Scott P., Venkatesan A., Roebber E., Gondolo P., Pierpaoli E., Holder G., 2011, ApJ, 742, 129
Seiffert M. et al., 2009, preprint (arXiv:0901.0559)
Sivertsson S., Gondolo P., 2011, ApJ, 729, 51
Spolyar D., Freese K., Gondolo P., 2008, Phys. Rev. Lett., 100, 051101
Spolyar D., Bodenheimer P., Freese K., Gondolo P., 2009, ApJ, 705, 1031
Steidel C. C., Giavalisco M., Pettini M., Dickinson M., Adelberger K. L., 1996, ApJ, 462, L17
Taoso M., Bertone G., Meynet G., Ekstrom S., 2008, Phys. Rev. D, 78, 123510
The Fermi LAT Collaboration, 2011, Phys. Rev. D, 84, 032007
Umeda H., Yoshida N., Nomoto K., Tsuruta S., Sasaki M., Ohkubo T., 2009, J. Cosmol. Astropart. Phys., 8, 24
Valluri M., Debattista V. P., Quinn T., Moore B., 2010, MNRAS, 403, 525
Venkatesan A., 2000, ApJ, 537, 55
Yoon S.-C., Iocco F., Akiyama S., 2008, ApJ, 688, L1
Yoshida N., Abel T., Hernquist L., Sugiyama N., 2003, ApJ, 592, 645
Zackrisson E., 2011, PoS, IDM2008, 085, SISSA, Trieste
Zackrisson E., Bergvall N., Leitet E., 2008, ApJ, 676, L9
Zackrisson E. et al., 2010a, ApJ, 717, 257
Zackrisson E. et al., 2010b, MNRAS, 407, L74
Zackrisson E., Rydberg C.-E., Schaerer D., Östlin G., Tuli M., 2011a, ApJ, 740, 13
Zackrisson E. et al., 2011b, MNRAS, 410, L57

This paper has been typeset from a TEX/LATEX file prepared by the author.